Article

Validation of Aerosol Products from AATSR and MERIS/AATSR Synergy Algorithms—Part 1: Global Evaluation

Yahui Che [1,2,†], Linlu Mei [3,*,†], Yong Xue [1,4], Jie Guang [1], Lu She [5], Ying Li [1,2], Andreas Heckel [6] and Peter North [6]

[1] The Key Laboratory of Digital Earth Science, Institute of Remote Sensing and Digital Earth, Chinese Academy of Sciences, Beijing 100094, China; 15011546747@163.com (Y.C.); yx9@hotmail.com (Y.X.); guangjier@163.com (J.G.); shelu_whu@163.com (L.S.); happyappleliying@163.com (Y.L.)
[2] University of Chinese Academy of Sciences, Beijing 100049, China
[3] Institute of Environmental Physics, University of Bremen, Otto-Hahn-Allee 1, 28359 Bremen, Germany
[4] Department of Computing and Mathematics, College of Engineering and Technology, University of Derby, Kedleston Road, Derby DE22 1GB, UK
[5] College of Resources and Environmental Science, Ningxia University, Yinchuan 750021, Ningxia Province, China
[6] Department of Geography, College of Science, Swansea University, Singleton Park, Swansea SA2 8PP, UK; a.heckel@swansea.ac.uk (A.H.); p.r.j.north@swansea.ac.uk (P.N.)
* Correspondence: mei@iup.physik.uni-bremen.de
† These authors contributed equally to this work.

check for
updates

Abstract: The European Space Agency's (ESA's) Aerosol Climate Change Initiative (CCI) project intends to exploit the robust, long-term, global aerosol optical thickness (AOT) dataset from Europe's satellite observations. Newly released Swansea University (SU) aerosol products include ATSR-2 (1995–2003) and AATSR (2002–2012) retrieval and synergy between AATSR and MERIS with a spatial resolution of 10 km. Recently an experimental version of a retrieval using AATSR/MERIS synergy was developed to provide four months of data for initial testing. In this study, both AATSR retrieval (SU/AATSR) and retrieval (SU/synergy) datasets are validated globally using Aerosol Robotic Network (AERONET) observations for March, June, September, and December 2008, as suggested by the Aerosol-CCI project. The analysis includes the impacts of cloud screening, surface parameterization, and aerosol type selections for two datasets under different surface and atmospheric conditions. The comparison between SU/AATSR and SU/synergy shows very accurate and consistent global patterns. The global evaluation using AERONET shows that the SU/AATSR product exhibits slightly better agreement with AERONET than the SU/synergy product. SU/synergy retrieval overestimates AOT for all surface and aerosol conditions. SU/AATSR data is much more stable and has better quality; it slightly underestimates fine-mode dominated and absorbing AOTs yet slightly overestimates coarse-mode dominated and non-absorbing AOTs.

Keywords: Aerosol-CCI; AATSR; AOT; global

1. Introduction

Due to the improvements of climate observation capabilities in the past half-century, especially regarding both passive and active satellite observations of both geostationary and polar-orbiting satellites, such observations are widely used in both regional and global applications [1]. Aerosol remote sensing is one of the most crucial aspects for global climate change researches. However,

only aerosol products that provide time series data of sufficient length, consistency, and continuity can be considered as potential suitable climate data records [2]. For instance, the Global Climate Observing System (GCOS) requires aerosol optical thickness (AOT) data with an accuracy of 0.01 [3]. Thus, intensive validation of satellite aerosol products is necessary before their further application.

High-quality aerosol remote sensing was initiated in the 1990s along with the development of new instruments [4]. The most popular satellite aerosol products are provided by the Moderate Resolution Imaging Spectrometer (MODIS), which includes three different aerosol retrieval algorithms: Dark-Target [5,6], Deep Blue [7], and MAIAC [8]. All three algorithms have been applied to its successor, the Visible Infrared Imaging Radiometer Suite (VIIRS) instrument. Additionally, a newly developed NOAA aerosol retrieval algorithm provides another aerosol product [9]. Instruments with multi-angles yield further possibilities for accurate aerosol retrievals, such as the Multiangle Imaging SpectroRadiometer (MISR) [10] and Advanced Along Track Scanning Radiometer (AATSR) [11–13].There are also three current aerosol retrieval algorithms for AATSR: the AATSR Dual View Algorithm (ADV) [14,15], Oxford-RAL Aerosol and Cloud (ORAC) [16], and Swansea University (SU) [17], all of which will be further used with the Sea and Land Surface Temperature Radiometer (SLSTR). Instruments such as the Ozone Monitoring Instrument (OMI) [18] and Polder [19] provide UV channels and/or polarization information to accurately retrieve the aerosol absorbing mode or aerosol fine mode fraction. Ocean color instruments like the Sea-Viewing Wide Field-of-View Sensor (SeaWIFS) and the MEdium Resolution Imaging Spectrometer (MERIS) are also useful for obtaining aerosol information. The MODIS DeepBlue algorithm was initially designed for SeaWIFS [7]. The newly developed eXtensible Bremen AErosol Retrieval (XBAER) [20,21] and European Space Agency (ESA) MERIS aerosol [22] provide two additional data sources for aerosol remote sensing.

Validation allows the data provider and user community to have a better understanding of the advantages and limitations of the dataset. It is scientifically incorrect to directly compare single satellite pixel observations to in situ point measurements due to the spatial and temporal scale differences. Ichoku et al. [23] proposed a method to compare the spatial statistics from satellite observations with the corresponding temporal statistics from in situ measurements to achieve a meaningful and balanced validation. The assumption is that the movement of air mass captured by a satellite in a spatial point of view will be sampled by in situ measurements during a certain period of time [23]. This validation strategy has been widely accepted and used in aerosol remote sensing.

Based on the method proposed by Ichoku et al. [23], intensive validations for MODIS aerosol products have been performed for Collection 4, 5, 5.1, and 6 [5,24–28]. From the validation results, MODIS aerosol retrieval algorithms have been improved for surface parameterization, aerosol type treatment, and cloud screening. The spatial resolution of aerosol products has also been improved from 10 km to 3 km while the coverage has been extended by combining different algorithms. Other instruments like MISR [29–31], SeaWiFS [32,33], and PARASOL [34,35] have been evaluated by Aerosol Robotic Network (AERONET) observations or inter-comparison with MODIS aerosol products or CALIOP observations.

European aerosol research has been driven by the ESA Aerosol-CCI project. This project is an intensive algorithm development effort that incorporates sensitivity analysis, validation, and inter-comparison activities, along with a round robin exercise of seven different retrieval algorithms [13]. Although ADV [14,15], ORAC [16], and SU [17,36] all have their advantages and disadvantages and an ensemble aerosol product has been proposed in the second phase of the project, validation of the SU algorithm indicated that it provides the overall best accuracy. Comparison of the three products with AERONET is given in [13], and detailed evaluation over China is given in [37]. Until now, there have been no published studies on the global inter-comparison of the Swansea AATSR aerosol product with the experimental synergy version.

This study aims to conduct a detailed validation for the two SU AOT datasets. The analysis includes a comparison between AATSR V4.21 and the synergy retrieval. Validation was performed using global AERONET data. The paper is organized as follows. The satellite and ground-based dataset are introduced in Section 2, the aerosol retrieval algorithms are described in Section 3, and the validation results and analysis are presented in Section 4.

2. Materials

2.1. AATSR

AATSR is a dual-view sensor on board the European Space Agency (ESA) satellite ENVISAT (May 2002–April 2012). It is the successor of ATSR-1 and ATSR-2 on board ERS-1 and ERS-2. AATSR provides unique dual-viewing (with a forward view angle of 55°) observation capabilities at different wavelengths and enables research into atmospheric properties and sea surface temperature, among others. AATSR data have an average swath of 500 km and a resolution of 1 km at the nadir, together with the following wavelengths: 0.55, 0.66, 0.87, 1.6, 3.7, 11, and 12 μm. The successor of AATSR is SLSTR onboard Sentinel-3, which was launched in February 2016.

2.2. MERIS

The MERIS instrument was onboard the same platform as AATSR on the European ENVISAT satellite (May 2002–April 2012); it has fifteen wavelength bands between 390 nm and 1040 nm with a programmable bandwidth between 2.5 nm and 30 nm. MERIS provides two different spatial resolutions; the full resolution is 300 m and the reduced resolution is 1 km with a swath width of 1150 km. Simultaneous observations of MERIS and AATSR enable the synergistic retrieval of different surface and atmospheric parameters. MERIS has a much wider swath and more wavelengths in the visible range than AATSR. Several channels in the blue wavelength, similar to the Sea-viewing Wide Field-of-view Sensor (SeaWiFS), provide the unique ability to retrieve aerosol information for both dark and bright surfaces [7]. However, information observed by the AATSR near-infrared channel (1.6 μm) can provide additional highly useful constraints for high-quality aerosol retrieval. The successor to MERIS is the OLCI instrument onboard Sentinel-3, launched on February 2016. Thus, synergy of MERIS/AATSR can be used on OLCI/SLSTR.

2.3. AERONET

AERONET is a globally distributed network of over 800 stations that provides standardized high-quality aerosol measurements, which are widely used in various aerosol-related studies, including satellite retrieval validation [38,39]. AERONET uses the CIMEL sun/sky radiometers to obtain direct sun and diffuse sky radiances within the 340–1020 nm and 440–1020 nm spectral ranges, respectively. AOT measurements are recorded every 15 min from direct solar radiation with an accuracy of 0.01–0.02 [38]. AERONET data can be downloaded from the official website (http://aeronet.gsfc.nasa.gov/). The AOT values at 550 nm are not directly provided by AERONET, but are interpolated from AERONET AOTs at 440 nm and 870 nm using the Ångström equation [40]. Figure 1 shows the AERONET site distributions.
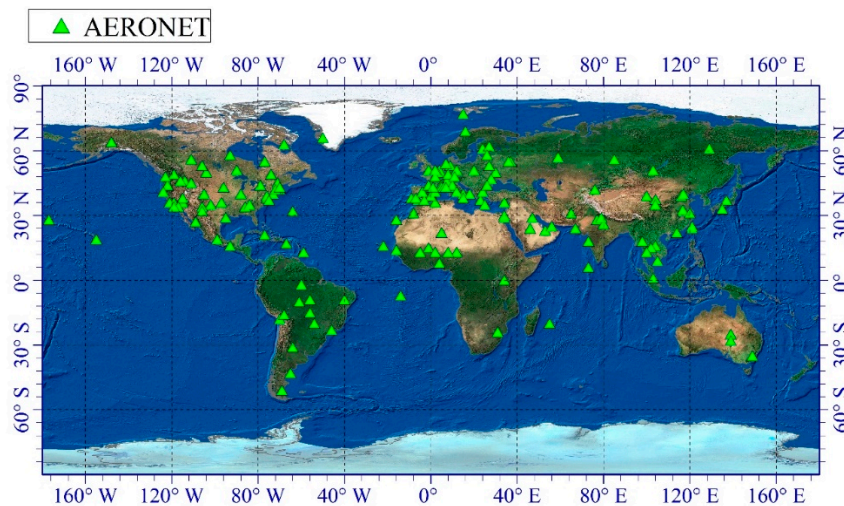
Figure 1. The spatial distribution of AERONET sites (green) used for validation.

3. Methods

3.1. AATSR Algorithm

The main advantage of the AATSR aerosol retrieval algorithm is to use its dual-view observation capability. As in the work of Veefkind and de Leeuw [41], for the AATSR aerosol retrieval used here, the ratio of surface reflectances at the nadir and forward observations has been correlated across wavebands, and the variation in surface anisotropy can be simply modelled using a surface parameterization model [42]. The dual-view avoids the need to obtain wavelength-dependent, accurate, and absolute surface reflectance values. This method differs from other approaches by using a more sophisticated physically based surface model to account for spectral variation of surface anisotropy owing to variations in of the fraction of scattered light with wavelength [42]. The retrieval uses a continuous mixture of the four basic aerosol components (dust, sea salt, weak-absorption, and strong-absorption) presented in de Leeuw et al. [11], in which dust and sea salt generally define the coarse mode and sulfate, organic matter, and black carbon define the fine mode. Additional information of the fine mode fraction and absorbing fine mode fraction is supplied in terms of monthly $1° \times 1°$ climatological data derived from two sources, modelling and observations in Kinne et al. [43]. The retrieval algorithm uses an iterative optimization of the AOT and aerosol model subject to multiple constraints (a multi-angular constraint over land and a spectral constraint over ocean) using a LUT method [17,36]. Uncertainty of the retrieved AOT is also provided using non-linear optimization of an error function, which considers the error from the surface model and observation errors from instrument calibration, the radiative transfer mode, and LUT (constructed by the radiative transfer code allowing rapid calculation of output parameters).

3.2. Synergy Algorithm

A version of the MERIS/AATSR synergistic algorithm for retrieval of aerosol properties has been described in detail by North et al. [44]. This was implemented in the ENVISAT BEAM processor, with intention to provide aerosol retrieval both as a product, and to allow atmospheric correction of both MERIS and AATSR data. This showed improvement over the equivalent single instrument algorithms in aerosol retrieval, though over a limited dataset, and intended to provide improvements over dark vegetated surfaces only. For the study presented here, a revised algorithm was developed to fit with compatible Aerosol CCI scheme and permitted to run over all surfaces to allow a global testing intended for further algorithm development... The synergy algorithm uses the combined wavelengths from both AATSR and MERIS observation, in which the aerosol types are defined the same as AATSR

algorithm. Substantial uncertainties in the retrieval of aerosol form multi angle or multi instrument measurements arise from errors in collocation of either forward to nadir images or images between different instruments. To compensate for these uncertainties it is useful to aggregate the individual measurements to 9×9 km^2 super pixels. This aggregation is done differently for AATSR and MERIS data as the two algorithm branches have different strength and weaknesses. For AATSR all cloud free pixels within the super pixel are averaged. For MERIS on the other hand only the 20 darkest pixels of the available cloud free pixels are used to compute an average TOA reflectance. The optimization is based on a linear combination of two separate error metrics for MERIS and AATSR data respectively, but with a consistent atmospheric composition. The spectral error metric used for MERIS is similar to the linear mixing model used in the Bremen AErosol Retrieval (BAER) algorithm [45]. The cloud screening algorithm employed here is classification approach developed by Gomez-Chova in the frame of the MERIS-AATSR-SYNERGY project [46]. This algorithm provides good results in detecting clouds for the nadir geometry where it benefits from the combined spectral band information of MERIS and AATSR. Unfortunately it does not provide a dedicated cloud mask for the forward view of AATSR. In the context of this option the derived cloud mask is extended by 3 pixels around each cloud to reduce the impact of this draw back. However cirrus or other clouds above an altitude of 4-5km are likely to provide contamination, leading to high bias, so the test dataset should be considered valid for cloud-free areas only. Over ocean, to provide a complete dataset, the same ocean surface model is used as for CCI, and retrieved using AATSR only, but using the MERIS/AATSR synergy cloud mask with twilight zone – differences over ocean indicate differences due to cloud masking only.

3.3. Major Differences between AATSR and AATSR/MERIS Synergy Algorithms

The main differences are summarized in Table 1. Due the instrument characteristic differences between AATSR and MERIS, as presented in Sections 2.1 and 2.2, the main differences between the two aerosol retrieval algorithms involve four aspects. The first part is the input difference. The AATSR algorithm uses four channels (0.55, 0.67, 0.87, and 1.6 µm) for both views while the synergy algorithm additionally uses 13 MERIS channels (all MERIS channels except 0.763 and 0.9 µm). The second aspect is the difference of cloud screening, which is the most important aspect for explaining the retrieval coverage difference. AATSR algorithm cloud screening is based on the ESA standard cloud mask and further improves the treatment for bright surfaces, thin clouds, and high aerosol loading cases by using new criteria. The synergy algorithm cloud mask is detailed in Gomez-Chova et al. [46], but applied to nadir only. The twilight zone effect [47] is considered by excluding three surrounding pixels to mask some residual cloud. The aerosol models are the same in AATSR and synergy algorithms, which is described in de Leeuw et al. [11]. However, the wavelength-dependent aerosol properties may play different roles in different retrievals. The difference in surface treatments due to the additional use of MERIS is a soil/vegetation mixture idea adapted from the Bremen AErosol Retrieval (BAER) algorithm. This idea has been used for MERIS surface parameterization [45].

Table 1. Differences between AATSR and synergy aerosol retrieval algorithms.

	AATSR	AATSR/MERIS
Input	AATSR R_{TOA} (0.55, 0.67, 0.87, and 1.6 μm) at both views	AATSR R_{TOA} (0.55, 0.67, 0.87, and 1.6 μm) at both views + all MERIS R_{TOA} (except 0.763 and 0.9 μm)
Cloud screening	Improved ESA standard cloud screening	Gomez-Chova [46] nadir only, + 3 pixels around excluded
Aerosol model	Aerosol-CCI defined [11]	Aerosol-CCI defined [11]
Surface model	North et al., 1999	North et al., 1999 + soil/vegetation mix
Limitations	Potentially operates at 2 km resolution, but usually degraded due to registration uncertainty Uses fixed set of aerosol models Not tested over snow/ice	Potentially operates at 2 km resolution, but usually degraded due to registration uncertainty uncertainty Not tested over snow/ice

3.4. Matchup Methodology

In situ measurements used as reference data, such as AERONET, provide a point measurement and have high temporal resolution (every 15 min), while satellites provide only a snapshot of a larger region in one pixel with different spatial resolutions at a single time. In order to consider both the spatial and temporal differences between satellite and in situ observations, the spatial-temporal collocation method proposed by Ichoku et al. [23] has been widely used in the aerosol community, which mitigates the effect of spatial/temporal variability. In this case, AERONET data averaged within 30 min of the AATSR/MERIS overpass are extracted and compared with AATSR/MERIS data averaged within a 25 km radius of the AERONET site. As AERONET does not conduct measurements at 550 nm, data are interpolated to 550 nm using the standard Ångström exponent.

3.5. Statistical Metrics

The MSA (Mean Satellite-retrieved AOT) and MAA (Mean AERONET AOT) are used to evaluate the differences between satellite-derived AOT and AERONET observed AOT. The relative mean bias (RMB) is defined as the ratio of MSA and MAA, which is an indicator of underestimation or overestimation for satellite-derived AOT. The MBE (mean bias error) and MAE (mean absolute-bias error) can be used as an indicator of the satellite-derived AOT bias. MAE can be used to show the scattering characteristics of the biases. All these statistical metrics can be used to evaluate the satellite-derived AOT. In this study, root-mean-square error (RMSE) and correlation coefficient (R) are also used as an important indicator, which are defined as

$$\text{MSA} = \frac{1}{n} \sum\nolimits_{i=1}^{n} \tau_{\text{sat,i}} \tag{1}$$

$$\text{MAA} = \frac{1}{n} \sum\nolimits_{i=1}^{n} \tau_{\text{AER,i}} \tag{2}$$

$$\text{RMB} = \text{MSA}/\text{MAA} \tag{3}$$

$$\text{MAE} = \frac{1}{n} \sum\nolimits_{i=1}^{n} |(\tau_{\text{sat,i}} - \tau_{\text{AER,i}})| \tag{4}$$

$$\text{MBE} = \frac{1}{n} \sum\nolimits_{i=1}^{n} (\tau_{\text{sat,i}} - \tau_{\text{AER,i}}) \tag{5}$$

$$\text{RMSE} = \sqrt{\left(\frac{1}{n} \sum\nolimits_{i=1}^{n} (\tau_{\text{sat,i}} - \tau_{\text{AER,i}})^2 \right)} \tag{6}$$

$$R(\tau_{sat}, \tau_{AER}) = \frac{Cov(\tau_{sat}, \tau_{AER})}{\sqrt{Var[\tau_{sat}]Var[\tau_{AER}]}} \tag{7}$$

where $Cov(\tau_{sat}, \tau_{AER})$ is the standard deviation of satellite-derived AOT and AERONET AOT and $Var[\tau_{sat}]$, $Var[\tau_{AER}]$ are the RMSE of satellite-derived AOT and AERONET AOT, respectively.

The classical linear regression analysis would lead to inestimable error if there are errors in variables, especially for the usage of prediction of material property in social science [48]. Other regression analysis such as orthogonal regression may have better performance than the standard linear regression [48]. In this paper, we do not perform standard regression analysis although it has been widely used for the validation of aerosol satellite products. Instead, EE is widely used to show the quality of aerosol satellite products. Chu et al. [25] validated MODIS AOT comparing AERONET AOT from 30 sites and proposed that MODIS retrievals should fall into an EE of $\pm 0.20 AOT_{AERONET} \pm 0.05$. On this basis, EE analysis was used in validation of MODIS Collection 003, 004, 005, and 6 [5,24,25,27] and narrowed from $\pm 0.20 AOT_{AERONET} \pm 0.05$ to $\pm 0.15 AOT_{AERONET} \pm 0.05$ [5,27]. Thus we define EE following the standard MODIS products validation as

$$EE = \pm 0.15 AOT_{AERONET} \pm 0.05 \tag{8}$$

4. Results

In this section, we present the evaluation results for SU AATSR and AATSR/MERIS synergy retrieval results. The data for the AATSR product can be downloaded from ICARE Data and Services Center (http://www.icare.univ-lille1.fr/). For the synergy dataset contact the author (p.r.j.north@swan.ac.uk). Because only four months of data (March, June, September, and December 2008) have been processed for AATSR/MERIS synergy retrieval, the global comparison will be performed for these four months.

4.1. Global AOT Pattern Comparison

The first step in comparing SU/AATSR and SU/synergy aerosol products is to analyze the global spatial distribution as it can provide an overview of the performance of different products, especially for major aerosol source regions like the anthropogenic pollution regions of India and eastern China, biomass burning regions in South Africa and South America, and desert and arid regions in North Africa and western China [49,50]. The AOT global distribution includes all possible cloud cover, aerosol, and surface types, which are the three aspects impacting retrieval quality. It also helps to explore how cloud screening and geometry co-register between different instruments and how different views impact data coverage and retrieval in different seasons. Additionally, the corresponding monthly averaged surface reflectance at 550 nm is used to understand the influence of surface reflectance on aerosol retrieval.

Figures 2a–5a (2a, 3a, 4a, 5a) present the monthly mean AOT of SU/AATSR and SU/synergy for March, June, September, and December 2008 while Figures 2c–5c shows the monthly averaged AOT difference. According to Figures 2a–5a, both algorithms show good performance, retrieving high AOT ($\tau > 0.6$) over North Africa, where the dominant aerosol is dust and biomass. Similar conclusions can be achieved for regions like South Asia, where aerosols are dominated by soot aerosols from biomass burning, urban emissions, or coal combustion. Almost no retrievals are provided for either dataset over regions with latitudes larger than 50°N in March and December. As well as the limited sunlight during these months, two other reasons may contribute: (1) the large sun zenith angle, which has been restricted to 70° in calculations using the lookup table (LUT) built by radiative transfer codes; (2) the significant snow cover in high-latitude regions, which cannot be retrieved for either proposed algorithm. It is interesting to note that the SU/synergy dataset has a larger coverage over high latitude regions than the SU/AATSR; however, the SU/AATSR product has a larger coverage over land than SU/synergy, especially over western China and Africa. This is mainly due to more conservative cloud screening in the SU/AATSR aerosol product, which will be described later. Besides the cloud

screening impact, the main reason involves differences of surface parameterization. According to Figures 2c–5c, SU/synergy generally provides higher AOT values than SU/AATSR; regions with a large AOT difference ($\Delta\tau > 0.1$) are concentrated in areas with high AOT loadings such as Africa, North India, and Eastern China. The patterns of AOT differences generally match AOT global distributions, indicating that absolute AOT differences increase with an increase of AOT. However, relatively large absolute AOT differences (over 0.1) are found in regions with relatively low AOT loading (AOT smaller than 0.3), such as Mexico, Southern South America, and South Africa. This may be due cloud cover, the complicated surface cover and high retrieval uncertainty due to less favourable solar view geometry in the southern hemisphere, where we sample the weaker aerosol backscatter from AATSR oblique view. Large predicted uncertainty in the retrieved AOT is also observed in the AOT uncertainty dataset provided by both algorithms.

SU/synergy generally shows higher global AOT than SU/AATSR. However, some lower SU/synergy AOTs are observed in northern South America, with limited sampling due to cloud screening. The second region is the Congo Basin, with AOT loading from 0.3 to 0.6. The third region is Australia, where the largest negative AOT values are found, with $\Delta\tau > 0.1$. The first and second regions are dominated by higher absorbing aerosol concentrations (biomass burning), indicating the potential impacts of aerosol type (especially the wavelength-dependent properties) in the two retrieval algorithms, despite using almost the same components as those proposed in the Aerosol-CCI project. The third region may further confirm the impact of aerosol typing because a large positive difference is observed between the Sahara Desert regions while a negative difference is observed over the Australian desert. Another potential impact may be attributed to the forward observation capability of AATSR, which may provide different 'information content' for southern and northern hemispheres. The 'information content' shows the capabilities of how precisely the proposed algorithm can retrieve the target parameters. The new retrieval using SLSTR shows the impact of changing the forward observations of AATSR to backward observations of SLSTR in the southern and northern hemisphere [44].

Figures 2d–5d show the monthly averaged surface reflectance at 550 nm for the selected months. It is clear that both two algorithms have the capability of retrieving AOT over bright surfaces (surface reflectance at 550 nm > 0.3). The absolute AOT differences generally follow the patterns of surface reflectance, which means that AOT differences increase with an increase of surface reflectance. This can be explained by the characteristics of the satellite aerosol retrieval algorithm linked to information content. Each surface type has a so-called critical surface reflectance (CSR), over which changes of AOT cannot influence TOA reflectance [51]. Dark surfaces increase aerosol sensitivity due to lower reflectance than CSR at each waveband, which enables retrieval over dark surfaces, generating AOT with a high information content. However, over a relatively bright surface, TOA reflectance is less sensitive to aerosol loading, especially for lower aerosol absorption values (e.g., desert regions), which have smaller wavelength-dependence features [50].
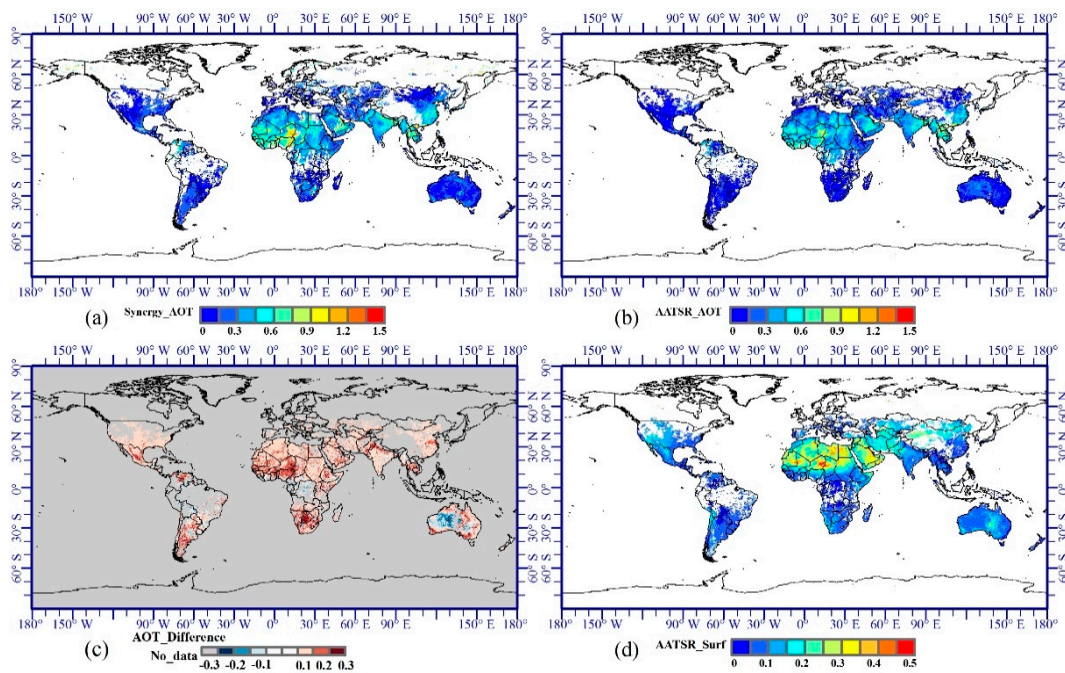
Figure 2. Global monthly averaged AOT difference between SU/synergy and SU/AATSR in March 2008. (**a**) Synergy AOT, (**b**) AATSR AOT, (**c**) AOT difference between synergy and AATSR, and (**d**) AATSR surface reflectance.
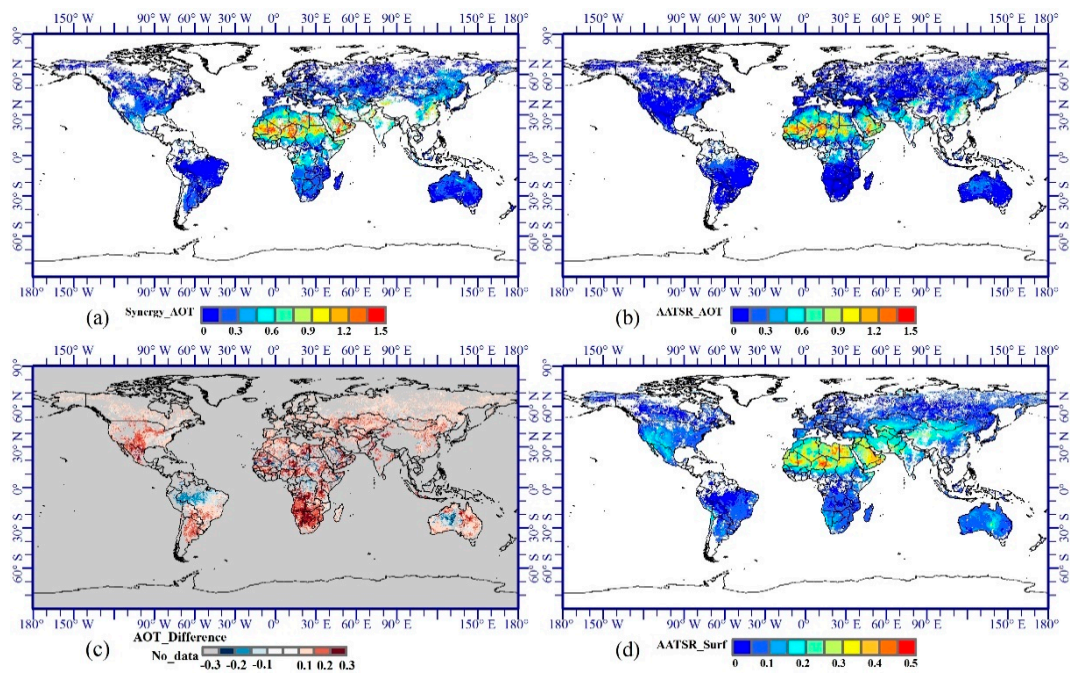
Figure 3. Global averaged monthly AOT difference between SU/synergy and SU/AATSR in June 2008. (**a**) Synergy AOT, (**b**) AATSR AOT, (**c**) AOT difference (synergy—AATSR), and (**d**) AATSR surface reflectance.

Aerosol types of high AOT quality are required for each month to understand the retrieval algorithm. March represents spring in the northern hemisphere. Both algorithms provide no retrieval over high latitudes, as shown in Figure 2a, due to snow cover or the high sun zenith angle, as well as cloud screening. For tropical areas such as Africa, the aerosol type is dominated by dust aerosols for Saharan areas [52] (surface reflectances at 550 nm > 0.3) and industrial and dust aerosols for most parts of South Africa [53]. In contrast, absorbing aerosols such as biomass burning dominate in northern South America [12], resulting in a negative AOT difference. Details of the AOT quality relating to aerosol absorption are discussed in Section 4.3.2. AOT differences in the Australian desert and surrounding coastal areas differ significantly from those in the Sahara Desert.

For June, retrievals over high latitude regions are greater for both algorithms than during March. No retrieval over western China and western America is observed by SU/AATSR in June. Further increases of AOT over North Africa are found for both datasets due to stronger dust plus biomass burning. This enhances changes in the AOT differences over North Africa, as shown in Figure 3c. Over southern North America and South Africa, where the aerosol source mainly constitutes urban emissions and industrial pollution, the AOT differences are larger than 0.1. As shown in Figure 3d, the surface reflectances in these areas are lower than 0.2, showing that the errors in aerosol typing may be the leading factor for the large AOT differences. Over northern South America and inland Australia, the AOT differences are still negative due to retrieval differences introduced by absorption aerosols. A mixture of dust aerosols and biomass burning in North and Central Africa results in both positive and negative AOT differences.

Compared to retrievals in June, one advantage of SU/synergy is its data coverage in September; more aerosol retrievals occur over high latitudes. SU/synergy AOTs show positive differences compared to individual SU/AATSR pixels, as shown in Figures 3a and 4b. The AOT differences decrease to 0.01–0.1 over the northern hemisphere. Over southern South America, most AOT differences are higher than 0.2 and the maximum AOT difference occurs over this area. Areas with negative AOT differences are the same as in other months over inland Australia, northern South America, and central Africa. The data coverage of AOT over northern South America is larger than that in March for both datasets.

In December, the AOT data coverage decreases from that in other months with movement of the sun zenith angle. AOT differences are lowest in all four months and almost all differences of pixels are in the range of 0.01–0.1. Examples of high AOT differences (larger than 0.1) exist over the southern hemisphere, especially southern South Africa, southern South America, and coastal areas of Australia.

In summary, AOTs derived from the SU/synergy algorithm are higher than those from SU/AATSR in most areas. Negative differences presented in Figures 2c, 3c, 4c and 5c tend to concentrate over central Africa, northern South America, and inland Australia. However, SU/AATSR AOTs are lower than SU/synergy AOTs over most areas except inland Australia, central Africa, and northern South America. This shows that the spatial distribution of overestimation is not consistent and has strong geographic patterns.
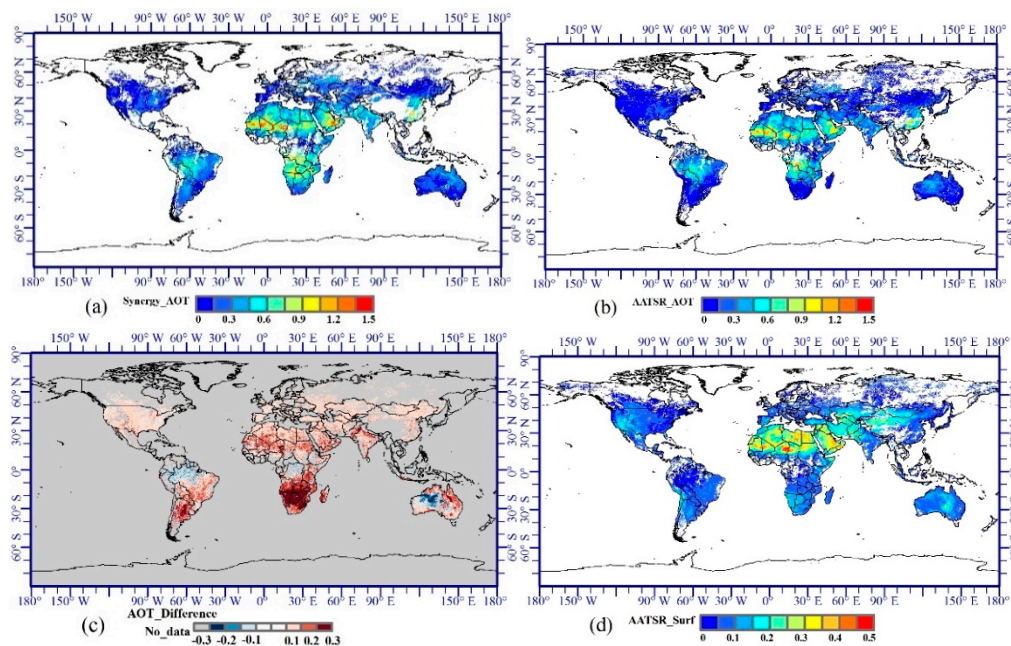
Figure 4. Global averaged monthly AOT difference between SU/synergy and SU/AATSR in September 2008. (**a**) Synergy AOT, (**b**) AATSR AOT, (**c**) AOT difference (synergy—AATSR), and (**d**) AATSR surface reflectance.
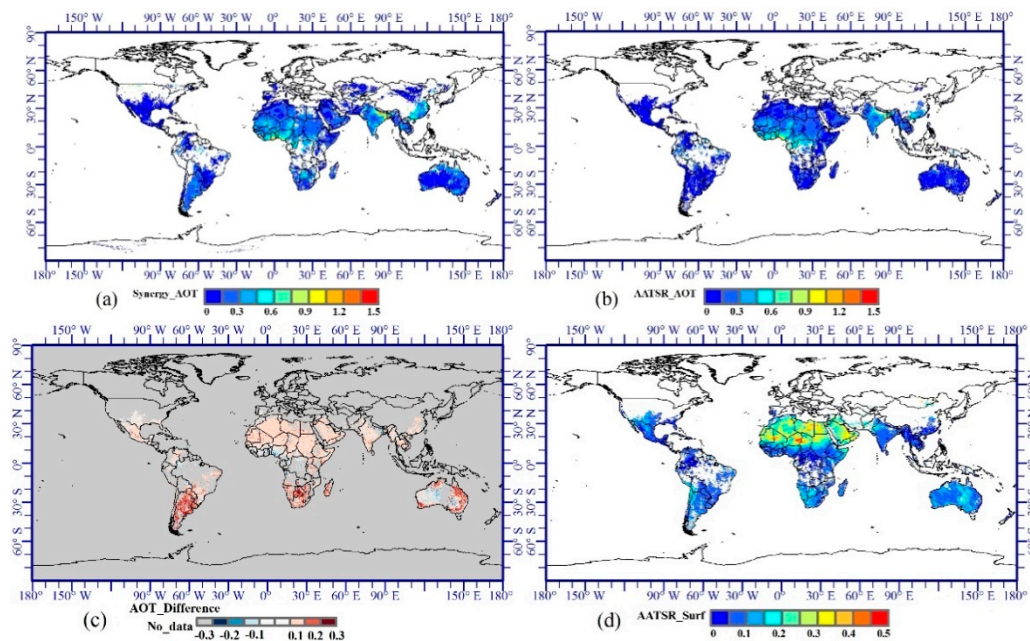
Figure 5. Global averaged monthly AOT difference between SU/synergy and SU/AATSR in December 2008. (**a**) Synergy AOT, (**b**) AATSR AOT, (**c**) AOT difference (synergy—AATSR), and (**d**) AATSR surface reflectance.

4.2. Global Validation Using AERONET

In Section 4.1, we qualitatively investigate the global difference between the two datasets. Here, we collocate all SU/synergy L2 AOT data of the selected four months in 2008 with the AERONET L2 dataset for a quantitative analysis. All collocated in situ stations are included in the analysis, as well as those in complicated coastal areas. Although aerosol retrieval around coastal areas may require

an additional separate analysis, as suggested by Wang et al. [54], we retain these match-ups in this analysis. Figure 6a,b show the spatial distribution of AERONET sites where ground-based data are used; the colors of each square indicate the match-up numbers of the collocation. In total, 742 matches are successfully collocated for the SU/AATSR product with AERONET datasets from 162 sites and 681 matches are successfully collocated for the SU/synergy data with AERONET datasets from 174 sites. The spatial distributions of AERONET sites with successful collocated matches are mainly determined by data quality and coverage of satellite-derived AOT. According to the collocation number, the data coverage of the SU/AATSR product is slightly larger than that of AATSR/synergy.
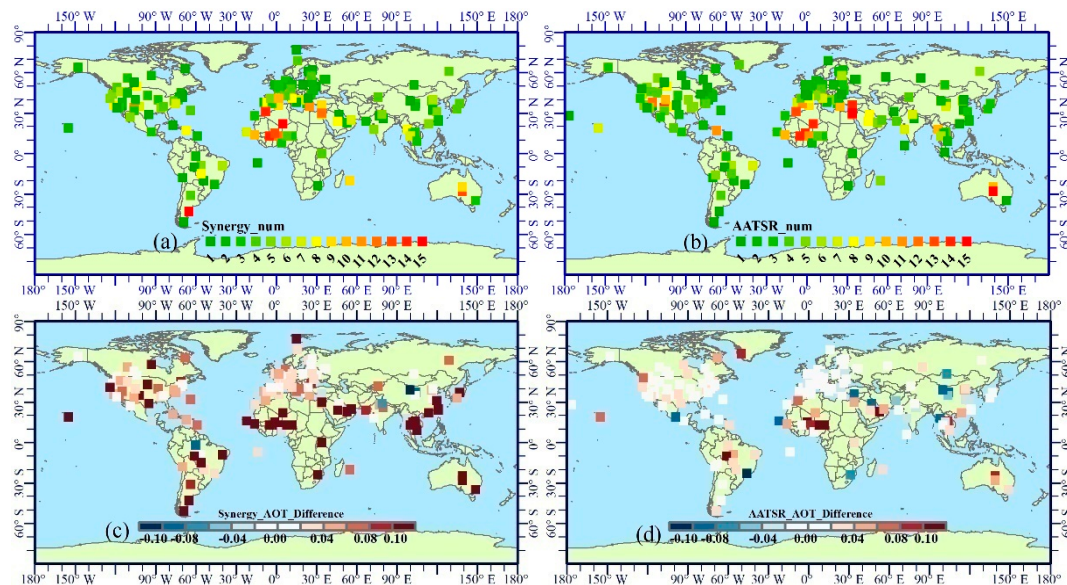
Figure 6. Global spatial distribution of collocated pairs and AOT differences between SU/synergy AOT and SU/AATSR AOT with AERONET datasets for each site in 2008. Spatial distribution of (**a**) synergy collocated pairs, (**b**) AATSR collocated pairs, (**c**) synergy AOT difference (synergy AOT—AERONET AOT), and (**d**) AATSR AOT difference (AATSR AOT—AERONET AOT).

Figure 6c,d reveals the spatial distribution of AOT biases of two datasets with respect to AERONET datasets. The SU/synergy algorithm overestimates AOT (MBE $\geq$ 0.10) for most sites in tropical areas (from the equator to 30°N), especially those in northern Africa and southeastern coastal China. On the other hand, it underestimates AOT over only a few sites, mainly in inland areas. However, SU/synergy generally performs well over areas with more AERONET sites (more match-ups); thus, on average, SU/synergy slightly overestimates AOT (MBE $\leq$ 0.04) over western Europe and most parts of North America. The performance of SU/AATSR is better than that of SU/synergy, in that no obvious overestimations or underestimations (except over desert regions) occur for most sites. AOT is overestimated over a few sites in northern Africa with an RMB value over 0.10.

Figure 7a,b illustrate scatter plots of AERONET L2 data with two AATSR datasets; the areas of each point represent the uncertainties of satellite retrieval (provided in the dataset) in each collocated pair and colors represent the standard deviation of AOTs in a 50 × 50 km sample area. The magenta points and lines are the mean and mean $\pm 2\sigma$ of satellite retrieved AOT in each AERONET AOT range (0.1), respectively. The dashed bold lines stand for Expected Error (EE) of $\pm 0.15 AOT_{AERONET} \pm 0.05$. We also plotted AOT histograms in the bottom right corner of each scatter plot to understand the distribution patterns of AOT biases. Basic statistics are included in the top left corner of each scatter box, including the number of collocated pairs, the correlation coefficient (R), the root mean square error (RMSE), and the percentages of matchups fall within, above, and below EE. R aims to find the fitting agreement between the two datasets. However, the correlation coefficient cannot be taken as

an independent metric of accuracy; thus, RMSE is introduced as the main evaluation metric together with R.
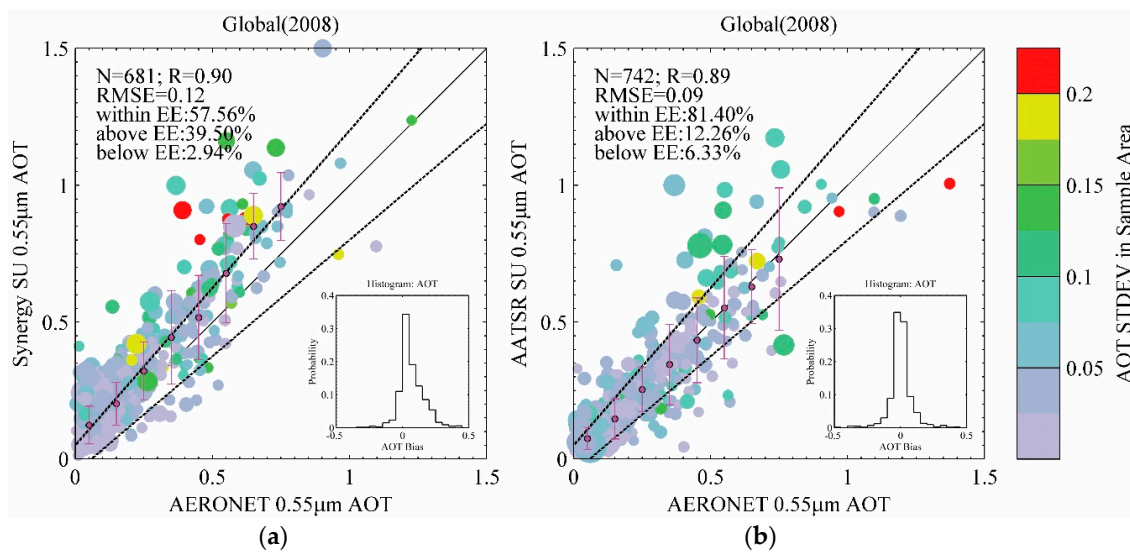
Figure 7. Scatter plots of AERONET L2 data with (**a**) SU/synergy and (**b**) SU/AATSR L2 AOT products in 2008. The colors of each point represent the AOT standard deviation in a sampling area measuring 50×50 km. Areas of each point represent the uncertainties of satellite retrieval (provided in the dataset) for each collocated pair. The magenta points and lines are the mean and mean $\pm 2\sigma$ of satellite retrieved AOTs in each AERONET AOT range (0.1). The dashed bold lines stand for expected error (EE) of $\pm 0.15 \text{AOT}_{\text{AERONET}} \pm 0.05$.

The uncertainty data in L2 datasets are included in the scatter plots to understand how the single pixel retrieval error contributes to the validation. The areas of most points (averaged retrieval uncertainties) are relatively small, indicating good qualities of both datasets in most cases. It should be noted that the colors of these scatter points do not represent the density but the standard deviation (Std) of retrieved AOT over a sampling area of 50×50 km. As well as the spatial variabilities of AOT, extremely large Stds may also reveal the influence of cloud contamination in particular for large spatial-window collocation [55], which plays a large role in the overestimation of AOT [56]. Points above the 1-1 lines of both datasets with Std values over 0.1 tend to be contaminated by residual cloud. From this point of view, the SU/AATSR dataset has a more homogenous AOT distribution and potentially better cloud mask processing because the colors of the points in Figure 7b are generally lighter than those in Figure 7a.

Detailed statistics of the comparison with AERONET are shown in Table A1. In total, SU/AATSR collocated 742 matches, more than the 681 matches of SU/synergy. This is mainly due to the different cloud screening of SU/synergy (discussed in Section 4.3.1). The four-month average values of MAA for both the SU/AATSR and SU/synergy are 0.19. A difference between MSAs for the SU/AATSR and SU/synergy occurs in the clear positive systematic error of SU/Synergy. It is obvious from Figure 7a,b that all magenta points lie above the 1-1 line, which is also indicated by the RMB value of 1.39 and the higher MSA value of 0.26. However, SU/AATSR does not exhibit overestimation, indicated by the fact that the MSA (0.20) of SU/AATSR is closer to the MAA (0.19), and the magenta points are distributed around the 1-1 line. According to Figure 7a, the performances of EE indicates overestimation of SU/synergy (39.5% vs. 12.26%). 39.50% of matchups fall above EE and only 2.94% of matchups fall below EE. Besides, SU/AATSR performs better than SU/synergy, indicated by 81.40% vs. 57.56% falling into EE.

In order to further understand the bias distribution patters related to AOT, we divide the AOT difference between satellite-derived and AEROENT AOTs into six classes: lower than −0.2, −0.2 to −0.1, −0.1 to 0, 0 to 0.1, 0.1 to 0.2, and higher than 0.2 (Table 2). The pixels in each class exhibit a continuous spatial distribution and strong geographic characteristics (Figures 2c–5c). The AOT differences between SU/synergy AOT and SU/AATSR AOT are presented in Table 2 using SU/AATSR as a reference. Most AOT differences fall into Class 3, ranging from 48.9% in June to 64.86% in December. The percentages of Class 2 and Class 5 are similar, as are those of Class 1 and Class 5. Negligible negative AOT differences are observed in Class 6 for all months. The best agreement between SU/synergy and SU/AATSR occurs in December. The percentage of Class 1 and Class 2 AOTs decreases to 2.86% and 10.16%, respectively. The percentage of Class 1 AOTs is 64.86% (maximum of all months).

Table 2. Fraction of AOT differences between SU/AATSR and SU/synergy and AERONET.

Classes	Range	March	June	September	December
Class 1	$\Delta\tau > 0.2$	4.38%	9.69%	9.64%	2.86%
Class 2	$0.2 \geq \Delta\tau > 0.1$	17.19%	20.05%	17.39%	10.16%
Class 3	$0.1 \geq \Delta\tau > 0$	61.53%	48.90%	57.63%	64.86%
Class 4	$0 \geq \Delta\tau > -0.1$	13.82%	15.32%	12.27%	20.89%
Class 5	$-0.1 \geq \Delta\tau > -0.2$	2.63%	4.62%	2.27%	1.13%
Class 6	$-0.2 \geq \Delta\tau$	0.45%	1.43%	0.79%	0.14%

To further investigate the biases of the two retrieval algorithms, comparisons were performed between SU/synergy, SU/AATSR, and AERONET observations for AOT difference ranges from above 0.1 to below 0.1. The results are presented as scatter plots in Figure 8. Figure 8a is the scatter plot of satellite AOT data with AERONET ground-based AOTs; the evaluation metrics are included in the upper left of each plot, including the number of total collocated points, the correlation coefficient, the RSME, and the fraction of EE. The statistical values between satellite-derived AOT and the two AOTs derived from the two algorithms are presented in Table 3. For the SU/AATSR AOT product, the accuracy of the algorithm (compared to AERONET data) shows minimal changes, with RMSE values from 0.079–0.098, R from 0.893–0.909, and fraction of match-ups fall into EE from 85.15% to 77.32% for $\Delta\tau \leq 0.1$ and $\Delta\tau > 0.1$, respectively. According to Figure 8b, we can see that SU/Synergy shows large overestimation especially for AOT bias larger than 0.1 compared to SU/AATSR (84.54% vs. 15.46%). Almost no underestimation from SU/synergy can be found while 7.22% from SU/AATSR is shown in Figure 8b, indicating the systematically error in surface parameterization in SU/synergy. This indicates that SU/AATSR produces stable AOT. However, the SU/synergy AOT dataset shows different features. RMSE values increase from 0.096–0.192 for $\Delta\tau \leq 0.1$ and $\Delta\tau > 0.1$, respectively. As mentioned before, SU/synergy shows systematic overestimation of AOT for the whole AOT range. We further compare these two satellite datasets with each other; very good correlations are observed with correlation coefficients of 0.990 and 0.979 for $\Delta\tau \leq 0.1$ and $\Delta\tau > 0.1$, respectively. The absolute differences between SU/synergy and SU/AATSR show a slight increase with an increase of AOT for $\Delta\tau \leq 0.1$. However, a systematic overestimation of approximately 0.12 is observed in Figure 8b.

Table 3. Comparison of statistical values between SU/AATSR, SU/synergy, and AERONET.

	Algorithm	N	R	RMSE	R_R	EE_w	EE_a	EE_b
$\Delta\tau \leq 0.1$	SU/synergy	330	0.894	0.096	0.990	69.39%	28.18%	2.42%
	SU/AATSR		0.893	0.079		85.15%	11.52%	3.33%
$\Delta\tau > 0.1$	SU/synergy	97	0.911	0.192	0.979	15.46%	84.54%	0
	SU/AATSR		0.909	0.098		77.32%	15.46%	7.22%
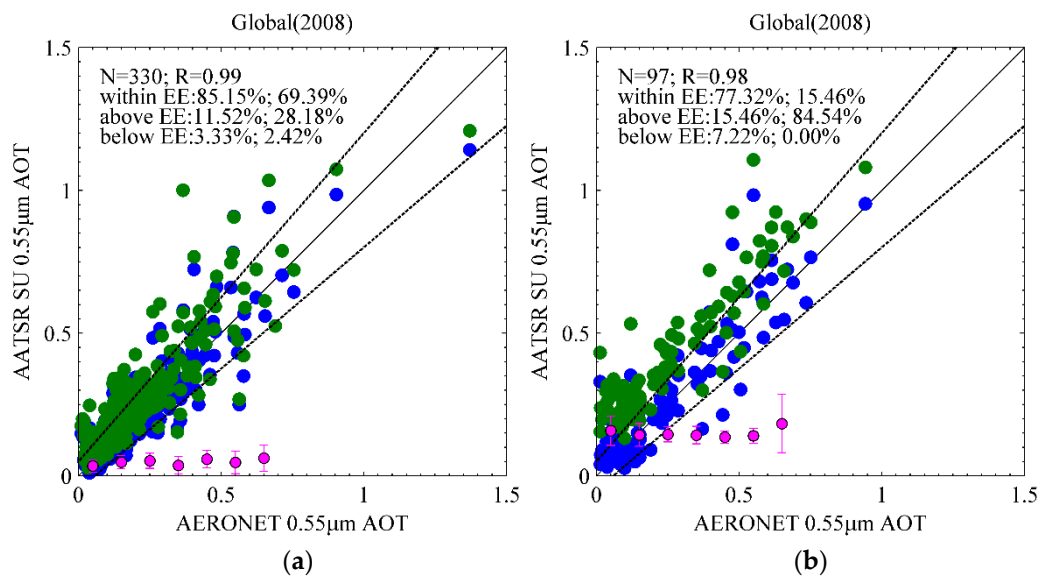
Figure 8. Scatter plot of SU/synergy AOT and SU/AATSR AOT with AERONET data for AOT ≤ bias < 0.1 (**a**) and AOT bias > 0.1 (**b**). Blue points represent SU/AATSR AOTs and green points represent SU/synergy AOTs. The magenta circles are the means of AOT difference in each range and lines of the same color are the means ± σ. The dashed bold lines stand for expected error (EE) of ±0.15AOT$_{AERONET}$ ± 0.05.

4.3. Factor Analysis

The following sections discuss the three most important factors: cloud screening, surface reflectance estimation, and aerosol typing, to qualitatively understand the two datasets according to their retrievals.

4.3.1. Cloud Screening

Figure 9 illustrates the differences between SU/AATSR and SU/synergy. AATSR has a swath width of approximately 500 km while the swath of MERIS is approximately 1150 km, more than twice that of AATSR (Figure 9c). However, due to the characteristic of the synergy dataset, only the overlap regions between MERIS and AATSR are used in the retrieval; thus, the advantage of the wide swath of MERIS is not applicable. It is more interesting that SU/synergy AOT sometimes shows lower coverage than SU/AATSR. Figure 9b,d show the AOT derived by SU/AATSR and SU/synergy over northeast China and Korea. The retrievals over North Korea (red rectangle) from SU/AATSR have much higher coverage than those of SU/synergy. According to the RGB figure presented in Figure 9a,c, the AOT spatial distribution from SU/AATSR agrees better with the cloud cover. According to RBG visualization, both MERIS and AATSR are cloud free, but SU/synergy AOT screens some 'non-cloudy' pixels. This is mainly because SU/synergy retrievals require that both AATSR (forward and nadir) and MERIS (nadir) are detected as cloud free, which further reduces the retrieval coverage. However, this indicates that SU/synergy is more likely to over-flag cloud than exhibit cloud contamination, in contrast to SU/AATSR, which means that the overestimation of SU/synergy is due to surface parameterization and aerosol typing.
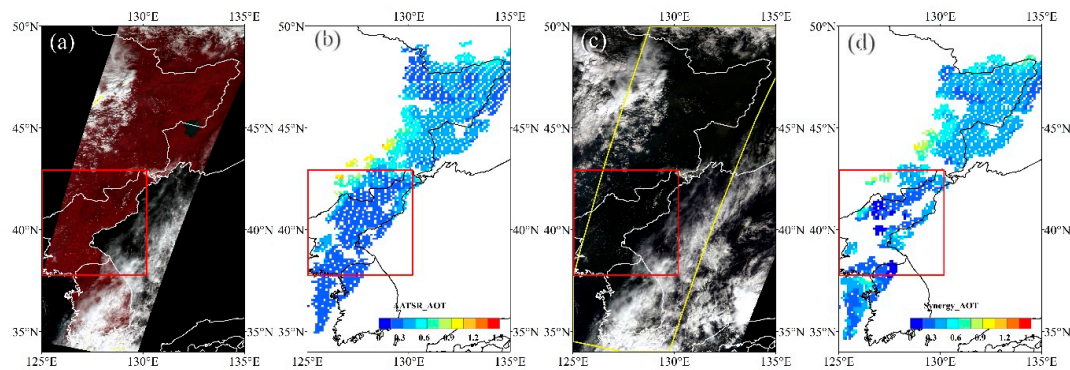
Figure 9. Influence of cloud masking in China and Korea: (**a**) AATSR RGB map, (**b**) SU/AATSR AOT, (**c**) MERIS RGB map, and (**d**) SU/synergy AOT.

4.3.2. Surface Reflectance

In this section, we perform a quantitative comparison of the two datasets with respect to surface reflectance. Note that this discussion assumes no influence of cloud contamination on all match-ups. Thus, the standard deviation of AOT in a sampling area ($0.5° \times 0.5°$) was selected as a threshold of 0.1 to minimize potential cloud contamination [15].

Figure 10 shows the scatter plots of SU/synergy and SU/AATSR biases with respect to SU/AATSR surface reflectance in the 550 nm wavelength, respectively. According to Figure 10a, SU/synergy overestimates AOT for almost all match-ups under all surface reflectance conditions. The best SU/synergy performances occur when surface reflectance is between 0.05 and 0.1. The average mean AOT bias for those cases is smaller than 0.05. When surface reflectance increases from 0.1 to 0.3, the AOT bias becomes larger, with a mean value of 0.2. Instability of the SU/synergy retrieval algorithm for each binned surface reflectance is reflected by the lengths of the magenta lines. The performance of SU/synergy deteriorates slightly with the increase of surface reflectance, especially for very bright surfaces where the reflectance at 550 nm is larger than 0.2. SU/AATSR typically shows no obvious overestimation or underestimation when the surface reflectance is less than 0.2. When the surface reflectance is more than 0.2, SU/AATSR tends to overestimate AOT with a bias from 0.05 to 0.1 (or above 0.3 in extreme cases, e.g., the Sahara Desert).
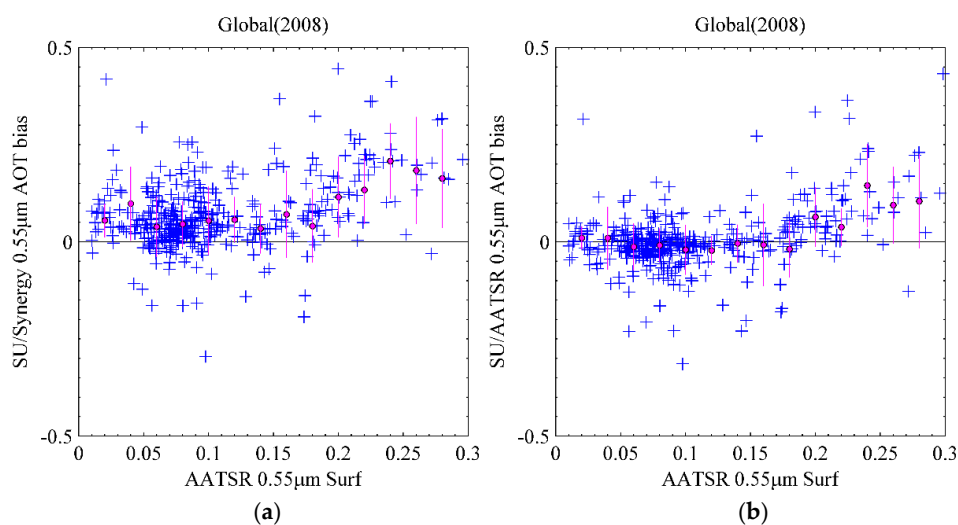
Figure 10. Scatter plots of SU/synergy (**a**) and SU/AATSR (**b**) bias with respect to SU/AATSR surface reflectance in the 550 nm wavelength. The magenta circles represent the means of AOT differences in each range and lines of the same color represent the means ± σ.

The box plots in Figure 11 present the seasonal characteristics of surface reflectance, AERONET AOT, SU/AATSR AOT, and SU/synergy AOT. In March, the surface reflectance at 550 nm changes from 0.09 to 0.16. Compared to the AERONET observed AOT, the box of SU/AATSR shows almost the same patterns as AERONET. A slight underestimate of high AOT and overestimate for low AOT is observed. The SU/synergy algorithm overestimates AOT for all surface reflectance values. In June, the changes of surface reflectance at 550 nm and AERONET AOT decrease. SU/AATSR shows a slight underestimate while SU/synergy overestimates AOT, similar to March. In September, the surface conditions are similar to June. The performance of SU/AATSR is good, and the box plot is almost the same as that for AERONET. The SU/synergy still overestimates AOTs. In December, the surface reflectance changes larger than in September. However, SU/synergy still overestimates AOT, but the minimum overestimate occurs in December.
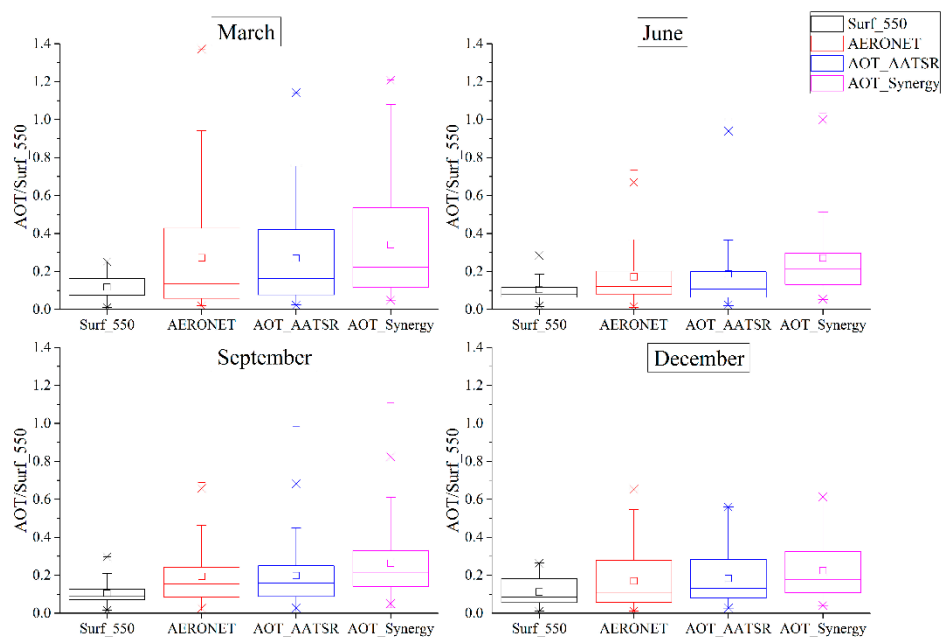
Figure 11. Seasonal comparison of surface reflectance at 550 nm for AERONET AOT, SU/AAYSR AOT, and SU/synergy AOT. For each box plot, the small square, 'x', and the 'bar above and below the box' represent the average value, 99% value, 1% value, maximum value, and minimum value of each group.

4.3.3. Aerosol Typing

Besides cloud screening and surface parameterization, aerosol typing is another important aspect that should be discussed. Figure 12a,b present the dependence of the SU/synergy bias (SU/synergy AOT—AERONET AOT) with respect to the Absorption AOT (AAOT) fraction and fine mode AOT (FAOT) fraction. Figure 13a,b show the SU/AATSR bias. As discussed previously, the SU/AATSR algorithm is generally more stable with respect to surface reflectance. Similar patterns are observed for aerosol absorbing and size parameters. Figure 13 is more concentrated and shows some regular patterns while Figure 12 exhibits no real patterns. Figure 12 shows that SU/synergy overestimates almost all aerosol types; however, SU/AATSR underestimates both absorbing aerosols and fine-mode dominated aerosols. Conversely, SU/synergy overestimates AOTs for both non-absorbing and coarse-mode dominated aerosols. For cases where AAOTs/AOTs are less than 0.05 (i.e., the dominant aerosol type is non-absorption aerosols), SU/synergy overestimates AOTs while SU/AATSR tends to underestimate AOTs. This may explain the large positive differences of AOT difference (between SU/synergy and SU/AATSR) over industrial areas (northern India, southern Africa, southern North America, and southern South America). For AAOT/AOT over 0.05, the SU/AATSR bias becomes positive, in contrast to smaller AAOT/AOT, and the differences of SU/AATSR and SU/synergy are comparable. This may

explain the negative differences in northern South America, central Africa, and the Australian desert in Figures 2c, 3c, 4c and 5c (blue color). Additionally, when the coarse mode dominates (FAOT/AOT less than 0.4), SU/AATSR tends to underestimate AOT; it then overestimates AOT as the FAOT/AOT increases. The SU/synergy algorithm exhibits hardly any regular patterns of AOT bias dependence with respect to the fine-mode fraction.
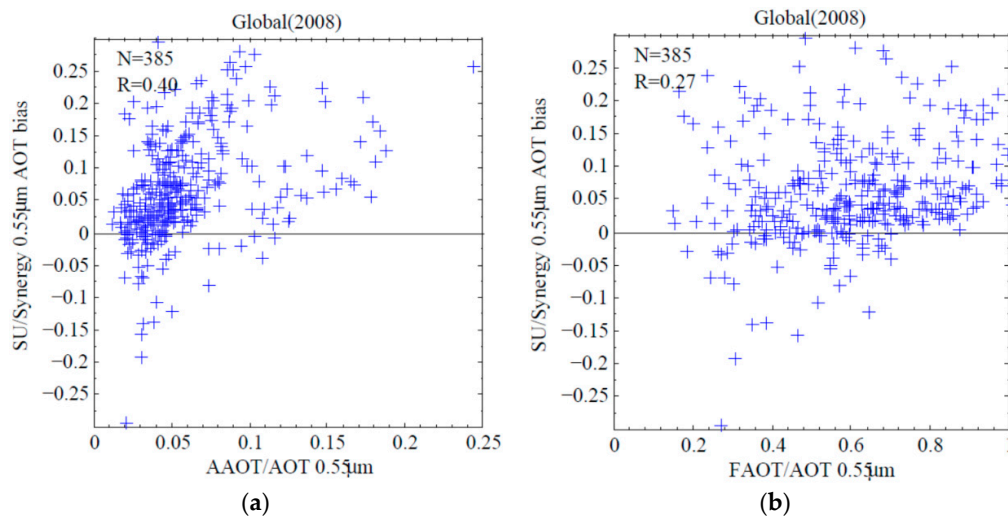
Figure 12. Scatter plots of (**a**) absorption aerosols/AERONET AOT with SU/synergy AOT bias and (**b**) fine-mode aerosols/AERONET AOT with SU/synergy AOT bias.
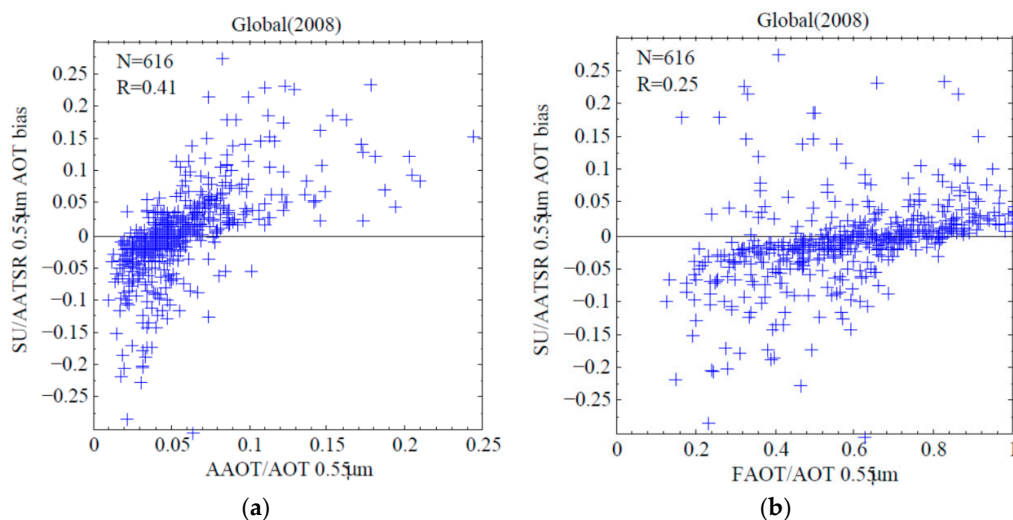
Figure 13. Scatter plots of (**a**) absorption aerosols/AERONET AOT with SU/AATSR AOT bias and (**b**) fine-mode aerosols/AERONET AOT with SU/AATSR AOT bias.

5. Conclusions

The SU AATSR V4.21 product was compared with an experimental retrieval developed by Swansea University using AATSR and MERIS data for March, June, September, and December 2008 as part of the Aerosol-CCI project. Future work includes (1) investigating of the data qualities over certain regions such as coast line and China; (2) the validation of the retrieval uncertainties, which will be a valuable dataset to analyze and provide a better understanding of the aerosol data.

AERONET data are selected as reference data to validate the two SU datasets. AERONET sites have an extremely uniform distribution over northern America and west Europe. Generally

speaking, AOT retrievals depend on cloud screening, surface parameterization, and aerosol typing. The SU/AATSR algorithm performs quite well for all AOTs over western Europe and northern America. However, the SU/synergy algorithm overestimates AOT over western Europe and northern America. This systematic error is predominantly caused by the surface assumptions and aerosol typing used in the algorithm. In order to further understand the systematic differences between the SU/synergy dataset and SU/AATSR dataset, the AOT difference maps between SU/synergy and SU/AATSR data were created for the four selected months. The AOT differences show strong geographical and seasonal characteristics. SU/synergy AOTs are higher than SU/AATSR AOTs, except over northern South America, central Africa, and inland Australia. Comparisons between SU/synergy, SU/AATSR, and AERONET observations further show the AOT quality of each retrieval. For cases where $\Delta\tau \leq 0.1$, the two algorithms have quite similar performances. However, for $\Delta\tau > 0.1$, SU/synergy performance deteriorates while the performance of SU/AATSR remains the same.

The data quality of the two retrievals was further evaluated for cloud screening, surface parameterization, and aerosol typing. SU/synergy shows stricter cloud screening than SU/AATSR, indicating less possibilities for cloud contamination. The overestimation of SU/synergy is due to both surface parameterization, especially for bright surfaces, and aerosol typing (for all aerosol sizes and absorption). SU/AATSR data quality is better than that of SU/synergy; indicated by underestimated fine-mode dominated aerosols and less absorbing AOTs, and vice versa for coarse-mode dominated and non-absorbing AOTs. In summary, for most vegetated areas, SU/AATSR shows good performance and SU/synergy tends to overestimate AOT for all (dark and bright) surfaces and aerosol conditions (different sizes and absorption characteristics). SU/AATSR underestimates AOT for biomass burning aerosols (absorption aerosols) and overestimates AOT for dust aerosols.

The comparison of validation results with the AERONET observations illustrates that the SU/AATSR algorithm exhibits better performance than the SU/synergy algorithm, since a positive bias was introduced in the synergy retrieval of AOD. A number of differences may explain this. The synergy algorithm .did not use explicit cloud screening for the oblique view, and angular component is based on an earlier version than the V4.21 product. Over ocean, despite using identical retrievals on AATSR only, the clear positive bias reported by the synergy algorithm indicates extensive cloud contamination due to lack of oblique view screening. In addition, the application of multiple instruments and multiple views introduces more errors, including those from co-registration between different datasetsg. Nevertheless, the synergy retrieval achieved similar or better overall correlation with AERONET, with R = 0.9 for synergy and R = 0.89 for the AATSR product. While some positive bias is explained due to incomplete cloud screening in the synergy processing, it is clear also that the initial surface spectra used for the spectral component of the retrieval need to be refined for future versions to reduce bias. This can be informed by similar work on spectral retrievals for MERIS and OLCI [20,50]. While ability to use full information from AATSR and MERIS ENVISAT instruments is demonstrated, further work is needed to improve treatment of surface spectra in particular to eliminate bias, and to prepare for implementation on OLCI/SLSTR on Sentinel-3.

the AERONET coordination team for organizing and maintaining excellent and essential support for satellite retrieval development and validation.

Conflicts of Interest: The authors declare no conflict of interest.

Appendix A
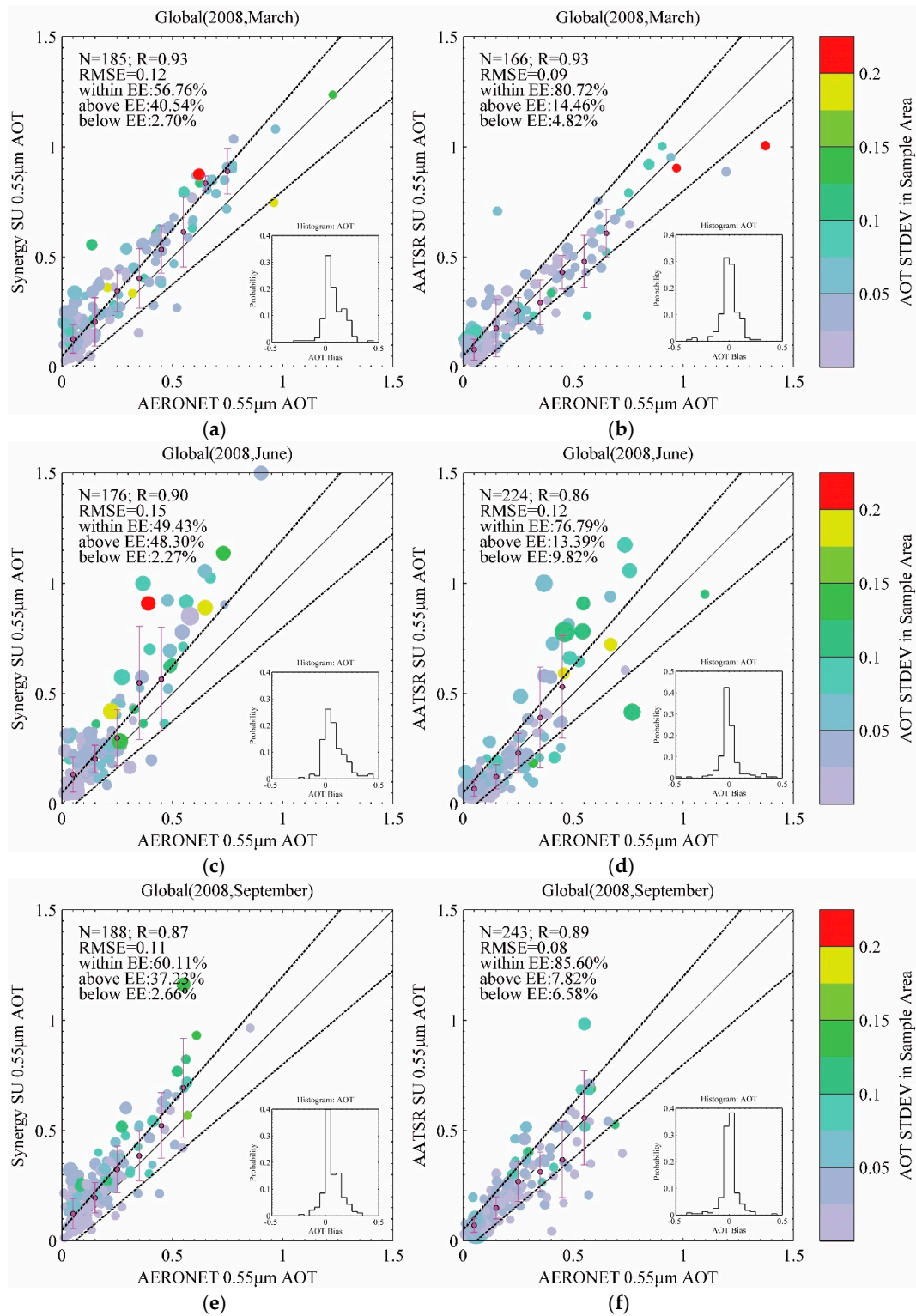
Figure A1. *Cont.*
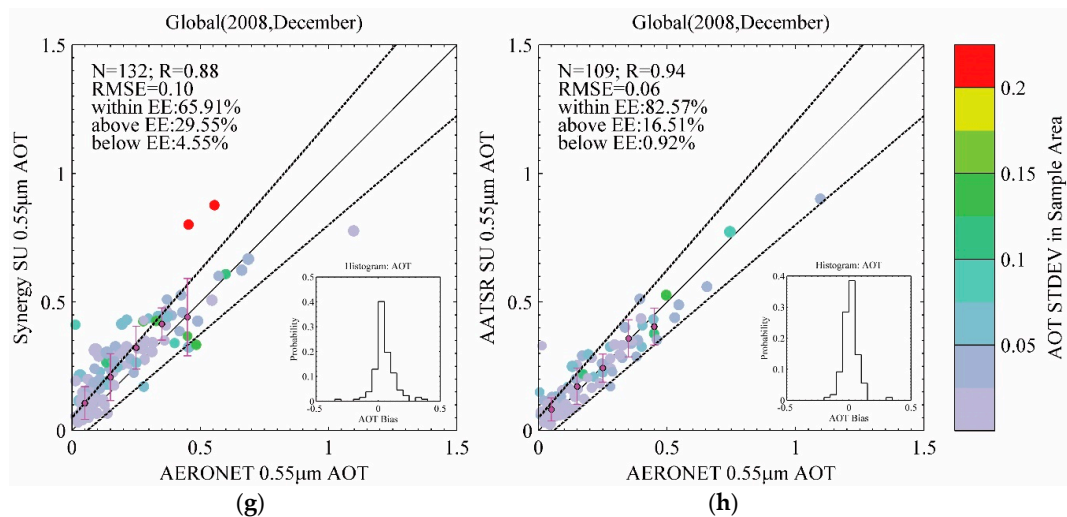
Figure A1. Seasonal (March, June, September, and December) scattering plots of AERONET data with SU/synergy and SU/AATSR data, 2008. (**a**) synergy AOT vs. AERONET AOT in March, (**b**) AATSR AOT vs. AERONET AOT in March, (**c**) synergy AOT vs. AERONET AOT in June, (**d**) AATSR AOT vs. AERONET AOT in June, (**e**) synergy AOT vs. AERONET AOT in September, (**f**) AATSR AOT vs. AERONET AOT in September, (**g**) synergy AOT vs. AERONET AOT in December, and (**h**) AATSR AOT vs. AERONET AOT in December.
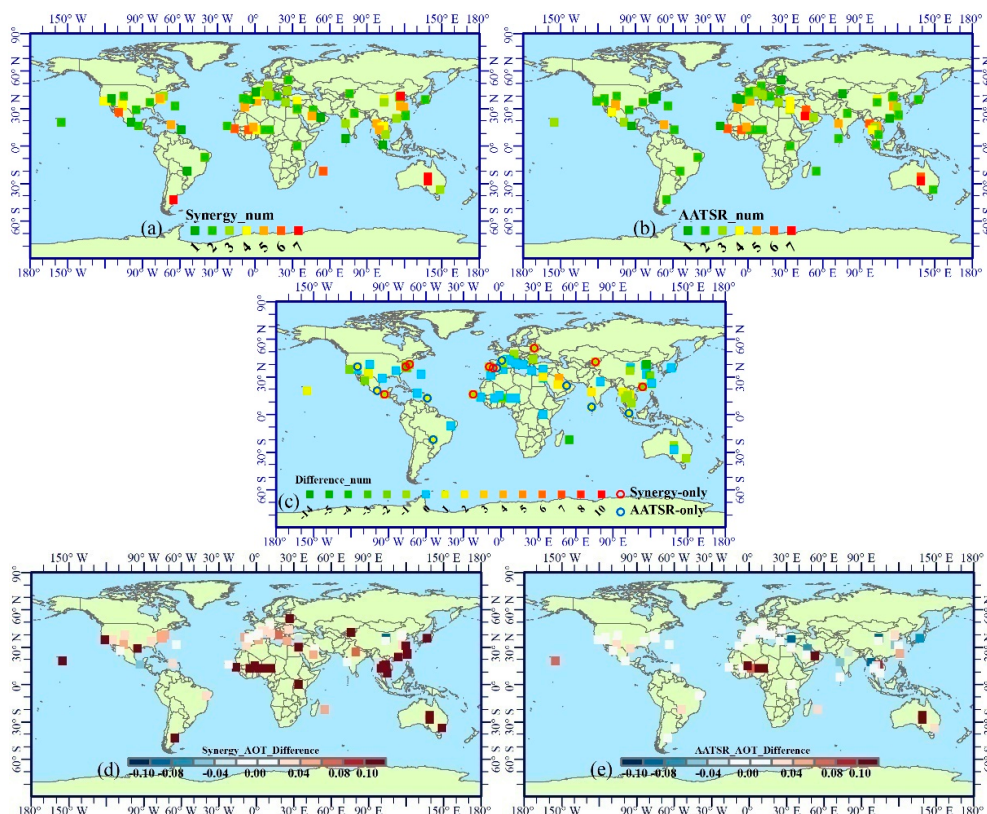
Figure A2. Global spatial distribution of collocated pairs and the AOT difference between SU/synergy AOT and SU/AATSR AOT with AERONET datasets for each site in March 2008. Spatial distributions of (**a**) synergy collocated pairs, (**b**) AATSR collocated pairs, (**c**) the synergy collocated pairs difference, (**d**) the synergy AOT difference (synergy AOT—AERONET AOT), and (**e**) the AATSR AOT difference (AATSR AOT—AERONET AOT).
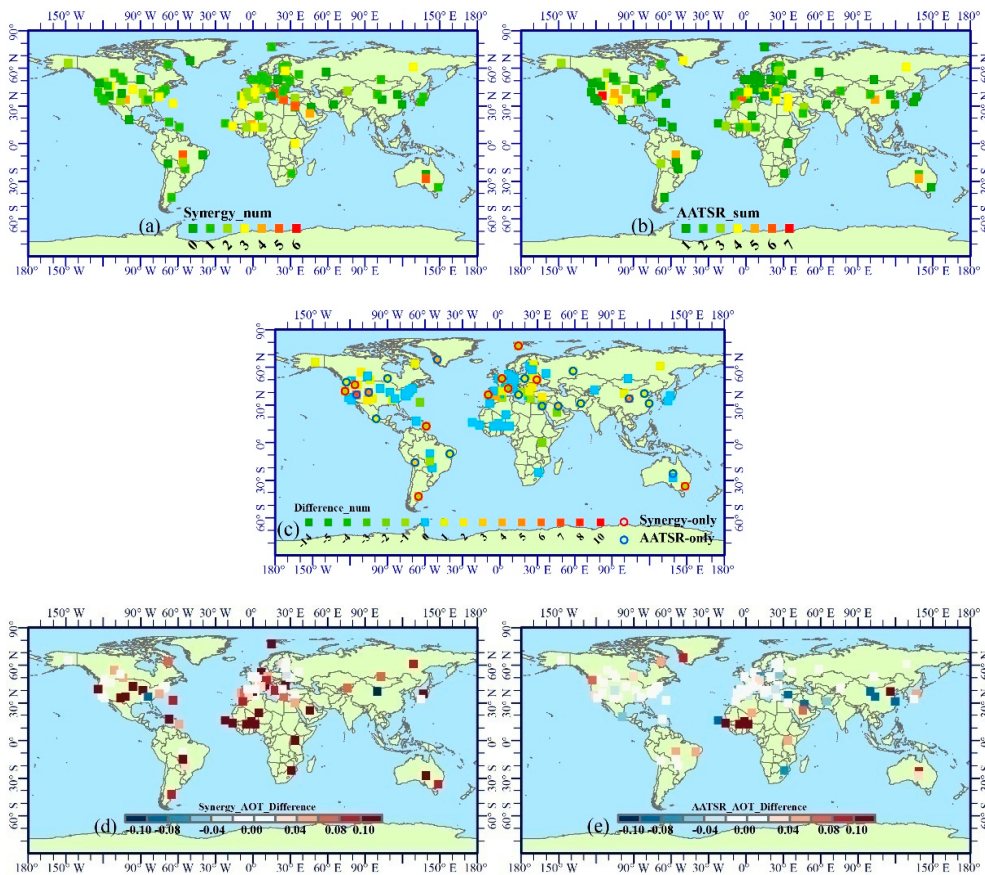
Figure A3. Global spatial distribution of collocated pairs and the AOT difference between SU/synergy AOT and SU/AATSR AOT with AERONET datasets for each site in June 2008. Spatial distributions of (**a**) synergy collocated pairs, (**b**) AATSR collocated pairs, (**c**) the synergy collocated pairs difference, (**d**) the synergy AOT difference (synergy AOT—AERONET AOT), and (**e**) the AATSR AOT difference (AATSR AOT—AERONET AOT).
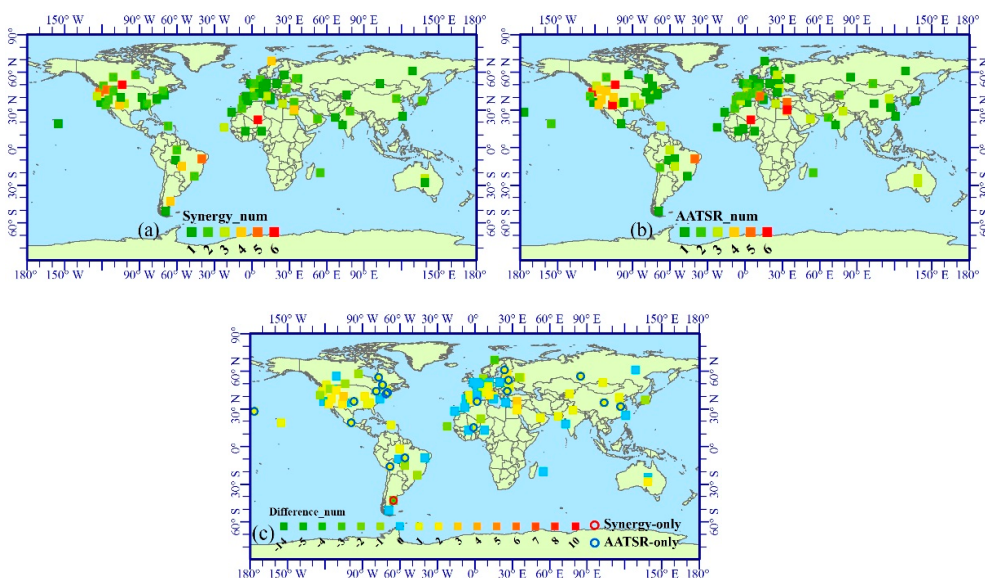
Figure A4. *Cont.*
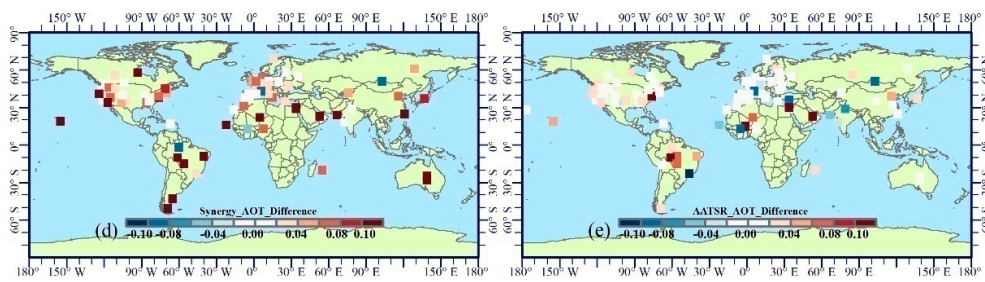
Figure A4. Global spatial distribution of collocated pairs and the AOT difference between SU/synergy AOT and SU/AATSR AOT with AERONET datasets for each site in September 2008. Spatial distributions of (**a**) synergy collocated pairs, (**b**) AATSR collocated pairs, (**c**) the synergy collocated pairs difference, (**d**) the synergy AOT difference (synergy AOT—AERONET AOT), and (**e**) the AATSR AOT difference (AATSR AOT—AERONET AOT).
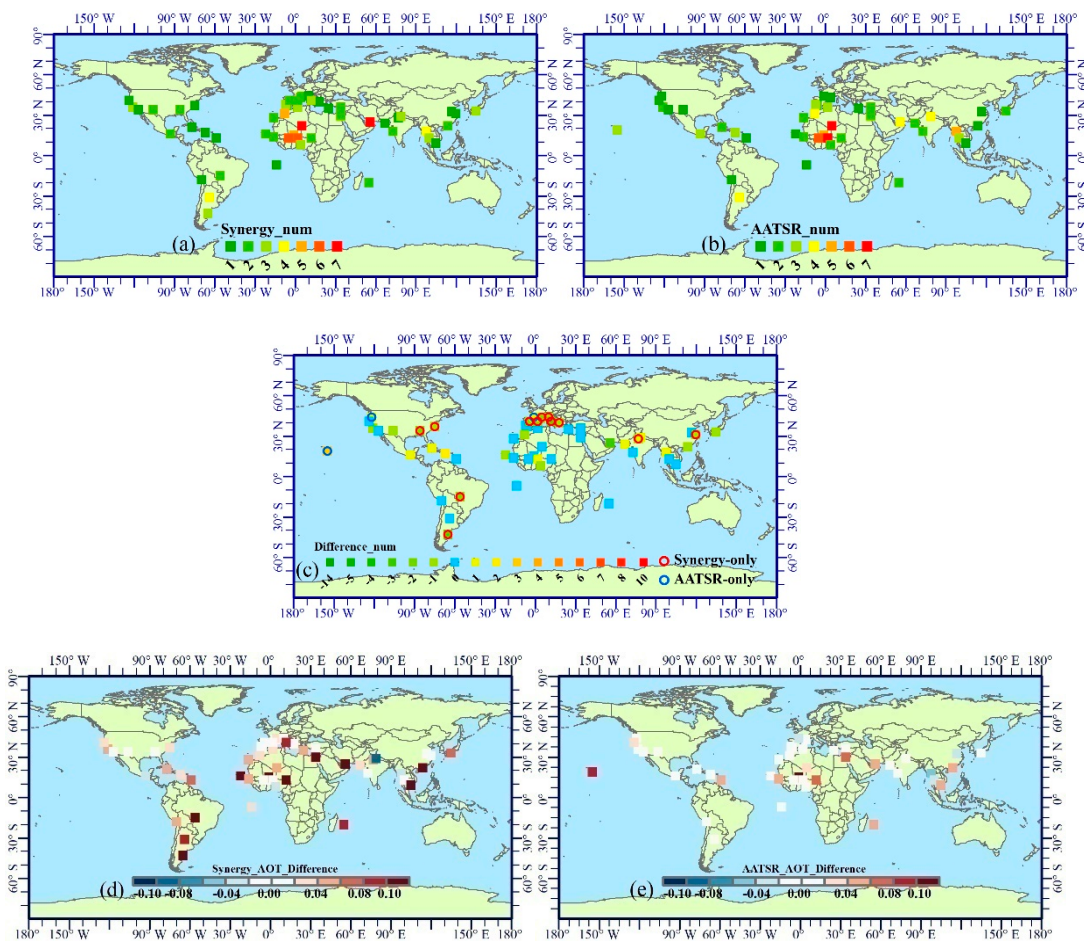
Figure A5. Global spatial distribution of collocated pairs and the AOT difference between SU/synergy AOT and SU/AATSR AOT with AERONET datasets for each site in December 2008. Spatial distributions of (**a**) synergy collocated pairs, (**b**) AATSR collocated pairs, (**c**) the synergy collocated pairs difference, (**d**) the synergy AOT difference (synergy AOT—AERONET AOT), and (**e**) the AATSR AOT difference (AATSR AOT—AERONET AOT).

Table A1. Validation statistics of SU/synergy and SU/AATSR AOT products.

		N	MSA	MAA	MBE	MAE	RMSE	RMB	EE_w	EE_a	EE_b	R
SU/AATSR	March	166	0.24	0.23	0.01	0.06	0.09	1.03	80.72%	14.46%	4.82%	0.93
	June	224	0.18	0.27	0.01	0.06	0.12	1.05	76.79%	13.39%	9.82%	0.86
	September	243	0.19	0.19	0.00	0.05	0.08	1.01	85.60%	7.82%	6.58%	0.89
	December	109	0.19	0.17	0.01	0.04	0.06	1.07	82.57%	16.51%	0.92%	0.94
	All	742	0.20	0.19	0.01	0.05	0.10	1.03	81.40%	12.26%	6.33%	0.89
SU/synergy	March	185	0.29	0.21	0.08	0.09	0.12	1.37	57.76%	40.54%	2.70%	0.94
	June	176	0.26	0.18	0.09	0.10	0.15	1.50	49.43%	48.30%	2.27%	0.90
	September	188	0.25	0.18	0.07	0.08	0.11	1.37	60.11%	37.23%	2.66%	0.87
	December	132	0.22	0.17	0.05	0.07	0.10	1.28	65.91%	29.55%	4.55%	0.88
	All	681	0.26	0.19	0.07	0.09	0.12	1.39	57.56%	39.50%	2.94%	0.90

References

1. Yang, W.; John, V.; Zhao, X.; Lu, H.; Knapp, K. Satellite climate data records: Development, applications and social benefits. *Remote Sens.* **2016**, *8*, 331. [CrossRef]
2. Peterson, T.C.; Baddour, O. Towards an enhanced climate system monitoring: Challenges and perspectives. *Clim. Res.* **2011**, *47*, 21–28. [CrossRef]
3. Global Climate Observing System (GCOS). *Systematic Observation Requirements for Satellite-Based Products for Climate—Supplemental Details to the Satellite-Based Component of the GCOS Implementation Plan*; Technical Report GCOS-107; WMO/TD No. 1338; GCOS: Springer: Berlin/Heidelberg, Germany, 2006.
4. Kaufman, Y.J.; Tanré, D.; Boucher, O. A satellite view of aerosols in the climate system. *Nature* **2002**, *419*, 215–223. [CrossRef] [PubMed]
5. Levy, R.C.; Mattoo, S.; Munchak, L.A.; Remer, L.A.; Sayer, A.M.; Patadia, F.; Hsu, N.C. The Collection 6 MODIS aerosol products over land and ocean. *Atmos. Meas. Tech.* **2013**, *6*, 2989–3034. [CrossRef]
6. Remer, L.A.; Mattoo, S.; Levy, R.C.; Munchak, L.A. MODIS 3 km aerosol product: Algorithm and global perspective. *Atmos. Meas. Tech.* **2013**, *6*, 1829–1844. [CrossRef]
7. Hsu, N.C.; Jeong, M.-J.; Bettenhausen, C.; Sayer, A.M.; Hansell, R.; Seftor, C.S.; Huang, J.; Tsay, S.-C. Enhanced Deep Blue aerosol retrieval algorithm: The second generation. *J. Geophys. Res. Atmos.* **2013**, *118*, 9296–9315. [CrossRef]
8. Lyapustin, A.; Wang, Y.; Laszlo, I.; Kahn, R.; Korkin, S.; Remer, L.; Levy, R.; Reid, J.S. Multiangle implementation of atmospheric correction (MAIAC): 2. Aerosol algorithm. *J. Geophys. Res. Atmos.* **2011**, *116*, D03211. [CrossRef]
9. Jackson, J.M.; Liu, H.; Laszlo, I.; Kondragunta, S.; Remer, L.A.; Huang, J.; Huang, H. Suomi-NPP VIIRS aerosol algorithms and data products. *J. Geophys. Res. Atmos.* **2013**, *118*, 12673–12689. [CrossRef]
10. Diner, D.J.; Martonchik, J.V.; Kahn, R.A.; Pinty, B.; Gobron, N.; Nelson, D.L.; Holben, B.N. Using angular and spectral shape similarity constraints to improve MISR aerosol and surface retrievals over land. *Remote Sens. Environ.* **2005**, *94*, 155–171. [CrossRef]
11. De Leeuw, G.; Holzer-Popp, T.; Bevan, S.; Davies, W.H.; Descloitres, J.; Grainger, R.G.; Griesfeller, J.; Heckel, A.; Kinne, S.; Klüser, L.; et al. Evaluation of seven European aerosol optical depth retrieval algorithms for climate analysis. *Remote Sens. Environ.* **2015**, *162*, 295–315. [CrossRef]
12. Holzer-Popp, T.; de Leeuw, G.; Griesfeller, J.; Martynenko, D.; Kluser, L.; Bevan, S.; Davies, W.; Ducos, F.; Deuze, J.L.; Graigner, R.G.; et al. Aerosol retrieval experiments in the ESA Aerosol_cci project. *Atmos. Meas. Tech.* **2013**, *6*, 1919–1957. [CrossRef]
13. Popp, T.; de Leeuw, G.; Bingen, C.; Bruehl, C.; Capelle, V.; Chedin, A.; Clarisse, L.; Dubovik, O.; Grainger, R.; Griesfeller, J.; et al. Development, Production and Evaluation of Aerosol Climate Data Records from European Satellite Observations (Aerosol_cci). *Remote Sens.* **2016**, *8*, 421. [CrossRef]
14. Sogacheva, L.; Kolmonen, P.; Virtanen, T.H.; Rodriguez, E.; Sundström, A.-M.; de Leeuw, G. Determination of land surface reflectance using the AATSR dual-view capability. *Atmos. Meas. Tech.* **2015**, *8*, 891–906. [CrossRef]
15. Kolmonen, P.; Sogacheva, L.; Timo, H.; Virtanen, T.H.; de Leeuw, G.; Kulmala, M. The ADV/ASV AATSR aerosol retrieval algorithm: Current status and presentation of a full-mission AOD dataset. *Int. J. Digit. Earth* **2016**, *9*, 545–561. [CrossRef]

16. Thomas, G.E.; Carboni, E.; Sayer, A.M.; Poulsen, C.A.; Siddans, R.; Grainger, R.G. Oxford-RAL Aerosol and Cloud (ORAC): Aerosol retrievals from satellite radiometers. In *Aerosol Remote Sensing over Land*; Kokhanovsky, A., de Leeuw, G., Eds.; Springer: Berlin/Heidelberg, Germany, 2009; pp. 193–225.

17. North, P.R.J. Estimation of aerosol opacity and land surface bidirectional reflectance from ATSR-2 dual-angle imagery: Operational method and validation. *J. Geophys. Res. Atmos.* **2002**, *107*, ACC4-1–ACC4-10. [CrossRef]

18. Torres, O.; Decae, R.; Veefkind, J.P.; de Leeuw, G. *OMI Algorithm Theoretical Basis Document Volume III Clouds, Aerosols, and Surface UV Irradiance*; NASA GSFC/University of Maryland: Baltimore, MD, USA, 2002; pp. 47–71.

19. Deuzé, J.; Bréon, F.; Devaux, C.; Goloub, P.; Herman, M.; Lafrance, B.; Maignan, F.; Marchand, A.; Nadal, F.; Perry, G.; et al. Remote sensing of aerosols over land surfaces from POLDER-ADEOS-1 polarized measurements. *J. Geophys. Res. Atmos.* **2001**, *106*, 4913–4926. [CrossRef]

20. Mei, L.L.; Rozanov, V.; Vountas, M.; Burrows, J.; Levy, R.; Lotz, W. Retrieval of aerosol optical properties using MERIS observations: Algorithm and some first results. *Remote Sens. Environ.* **2017**, *197*, 125–140. [CrossRef] [PubMed]

21. Mei, L.L.; Rozanov, V.; Vountas, M.; Burrows, J.; Levy, R.; Lotz, W. A Cloud masking algorithm for the XBAER aerosol retrieval using MERIS data. *Remote Sens. Environ.* **2017**, *197*, 141–160. [CrossRef]

22. Santer, R.; Carrere, V.; Dubuisson, P.; Roger, J.C. Atmospheric correction over land for MERIS. *Int. J. Remote Sens.* **1999**, *20*, 1819–1840. [CrossRef]

23. Ichoku, C.; Chu, D.A.; Mattoo, S.; Kaufman, Y.J.; Remer, L.A.; Tanré, D.; Slutsker, I.; Holben, B.N. A spatio-temporal approach for global validation and analysis of MODIS aerosol products. *Geophys. Res. Lett.* **2002**, *29*, MOD1-1–MOD1-4. [CrossRef]

24. Remer, L.A.; Kaufman, Y.J.; Tanre, D.; Mattoo, S.; Chu, D.A.; Martins, J.V.; Li, R.R.; Ichoku, C.; Levy, R.C.; Kleidman, R.G.; et al. The MODIS aerosol algorithm, products and validation. *J. Atmos. Sci.* **2005**, *62*, 947–973. [CrossRef]

25. Chu, D.; Kaufman, Y.; Ichoku, C.; Remer, L.; Tanré, D.; Holben, B. Validation of MODIS aerosol optical depth retrieval over land. *Geophys. Res. Lett.* **2002**, *29*, MOD2-1–MOD2-4. [CrossRef]

26. Li, Z.; Niu, F.; Lee, K.-H.; Xin, J.; Hao, W.; Nordgren, B.; Wang, Y.; Wang, P. Validation and understanding of Moderate Resolution Imaging Spectroradiometer aerosol products (C5) using ground-based measurements from the handheld Sun photometer network in China. *J. Geophys. Res. Atmos.* **2007**, *112*, D22S07. [CrossRef]

27. Levy, R.C.; Remer, L.A.; Kleidman, R.G.; Mattoo, S.; Ichoku, C.; Kahn, R.; Eck, T.F. Global evaluation of the Collection 5 MODIS dark-target aerosol products over land. *Atmos. Chem. Phys.* **2010**, *10*, 10399–10420. [CrossRef]

28. Sayer, A.M.; Hsu, N.C.; Bettenhausen, C.; Jeong, M.-J. Validation and uncertainty estimates for MODIS Collection 6 "Deep Blue" aerosol data. *J. Geophys. Res. Atmos.* **2013**, *118*, 7864–7872. [CrossRef]

29. Kahn, R.A.; Gaitley, B.J.; Martonchik, J.V.; Diner, D.J.; Crean, K.A. Multiangle Imaging Spectroradiometer (MISR) global aerosol optical depth validation based on 2 years of coincident Aerosol Robotic Network (AERONET) observations. *J. Geophys. Res. Atmos.* **2005**, *110*, D10S04. [CrossRef]

30. Kahn, R.A.; Li, W.H.; Moroney, C.; Diner, D.J.; Martonchik, J.V.; Fishbei, E. Aerosol source plume physical characteristics from Space-based multiangle imaging. *J. Geophys. Res. Atmos.* **2007**, *112*, D11205. [CrossRef]

31. Kahn, R.A.; Nelson, D.L.; Garay, M.J.; Levy, R.C.; Bull, M.A.; Diner, D.J.; Martonchik, J.V.; Paradise, S.R.; Hansen, E.G.; Remer, L.A. MISR aerosol product attributes and statistical comparisons with MODIS. *IEEE Trans. Geosci. Remote Sens.* **2009**, *47*, 4095–4114. [CrossRef]

32. Sayer, A.M.; Hsu, N.C.; Bettenhausen, C.; Ahmad, Z.; Holben, B.N.; Smirnov, A.; Thomas, G.E.; Zhang, J. SeaWiFS Ocean Aerosol Retrieval (SOAR): Algorithm, validation, and comparison with other data sets. *J. Geophys. Res. Atmos.* **2012**, *117*, 812–819. [CrossRef]

33. Sayer, A.M.; Hsu, N.C.; Bettenhausen, C.; Jeong, M.J.; Holben, B.N.; Zhang, J. Global and regional evaluation of over-land spectral aerosol optical depth retrievals from SeaWiFS. *Atmos. Meas. Tech.* **2012**, *5*, 1761–1778. [CrossRef]

34. Goloub, P.; Tanre, D.; Deuze, J.L.; Herman, M.; Marchand, A.; Breon, F.-M. Validation of the first algorithm applied for deriving the aerosol properties over the ocean using the POLDER/ADEOS measurements. *IEEE Trans. Geosci. Remote Sens.* **2002**, *37*, 1586–1596. [CrossRef]

35. Tanré, D.; Bréon, F.M.; Deuzé, J.L.; Dubovik, O.; Ducos, F.; François, P.; Goloub, P.; Herman, M.; Lifermann, A.; Waquet, F. Remote sensing of aerosols by using polarized, directional and spectral measurements within the A-Train: The PARASOL mission. *Atmos. Meas. Tech.* **2011**, *4*, 1383–1395. [CrossRef]

36. Bevan, S.; North, P.; Los, S.; Grey, W. A global dataset of atmospheric aerosol optical depth and surface reflectance from AATSR. *Remote Sens. Environ.* **2012**, *116*, 199–210. [CrossRef]

37. Che, Y.; Xue, Y.; Mei, L.; Guang, J.; Xu, H.; She, L.; Guo, J.; He, X.; Di, A.; Fan, C. Inter-comparison of three AATSR Level 2 (L2) AOD products over China. *Atmos. Chem. Phys.* **2016**, *16*, 9655–9674. [CrossRef]

38. Holben, B.N.; Eck, T.F.; Slutsker, I.; Tanré, D.; Buis, J.P.; Setzer, K.A.; Vermote, E.; Reagan, J.A.; Kaufman, Y.J.; Nakajima, T.; et al. AERONET—A Federated Instrument Network and Data Archive for Aerosol Characterization. *Remote Sens. Environ.* **1998**, *66*, 1–16. [CrossRef]

39. Holben, B.N.; Tanré, D.; Smirnov, A.; Eck, T.F.; Slutsker, I.; Abuhassan, N.; Newcomb, W.W.; Schafer, J.S.; Chatenet, B.; Lavenu, F.; et al. An emerging ground-based aerosol climatology: Aerosol optical depth from AERONET. *J. Geophys. Res. Atmos.* **2001**, *106*, 12067–12097. [CrossRef]

40. Ångström, A. Solar and terrestrial radiation. Report to the international commission for solar research on actinometric investigations of solar and atmospheric radiation. *Q. J. R. Meteorol. Soc.* **1924**, *50*, 121–126. [CrossRef]

41. Veefkind, J.P.; de Leeuw, G.; Durkee, P.A. Retrieval of aerosol optical depth over land using two-angle view satellite radiometry during TARFOX. *Geophys. Res. Lett.* **1998**, *25*, 3135–3138. [CrossRef]

42. North, P.R.J.; Briggs, S.A.; Plummer, S.E.; Settle, J.J. Retrieval of land surface bidirectional reflectance and aerosol opacity from ATSR-2 multiangle imagery. *IEEE Trans. Geosci. Remote Sens.* **1999**, *37*, 526–537. [CrossRef]

43. Kinne, S.; Schulz, M.; Textor, C.; Guibert, S.; Balkanski, Y.; Bauer, S.; Berntsen, T.; Berglen, T.; Boucher, O.; Chin, M.; et al. An AeroCom initial assessment optical properties in aerosol component modules of global models. *Atmos. Chem. Phys.* **2006**, *6*, 1815–1834. [CrossRef]

44. North, P.; Grey, W.; Heckel, A.; Fischer, J.; Preusker, R.; Brockmann, C. *MERIS/AATSR Synergy Algorithms for Cloud Screening, Aerosol Retrieval, and Atmospheric Correction*; ESRIN Contract No. 21090/07/I-LG; Algorithm Theoretical Basis Document Land Aerosol and Surface Reflectance ATBD; Swansea University: Swansea, UK, 2010.

45. Von Hoyningen-Huene, W.; Joon, Y.; Vountas, M.; Istomina, G.; Rohen, G.; Dinter, T.; Kokhanovsky, A.; Burrows, J. Retrieval of spectral aerosol optical thickness over land using ocean colour sensors MERIS and SeaWiFS. *Atmos. Meas. Tech.* **2011**, *4*, 151–171. [CrossRef]

46. Gomez-Chova, L.; Camps-Valls, G.; Calpe, J.; Munoz, J.; Moreno, J. *MERIS/AATSR Synergy Algorithms for Cloud Screening, Aerosol Retrieval, and Atmospheric Correction: Cloud Screening ATBD, version 1.0*; University of Valencia: Valencia, Spain, 2010.

47. Koren, I.; Remer, L.A.; Kaufman, Y.J.; Rudich, Y.; Martins, J.V. On the twilight zone between clouds and aerosols. *Geophys. Res. Lett.* **2007**, *34*, 162–179. [CrossRef]

48. Keleş, T. Comparison of Classical Least Squares and Orthogonal Regression in Measurement Error Models. *Int. Online J. Educ. Sci.* **2018**, *10*, 200–214.

49. Mei, L.L.; Rozanov, V.; Vountas, M.; Burrows, J.P. The retrieval of ice cloud parameters from multi-spectral satellite observations of reflectance using a modified XBAER algorithm. *Remote Sens. Environ.* **2018**, *215*, 128–144. [CrossRef]

50. Mei, L.L.; Rozanov, V.; Vountas, M.; Burrows, J.P.; Richter, A. XBAER-derived aerosol optical thickness from OLCI/Sentinel-3 observation. *Atmos. Chem. Phys.* **2018**, *18*, 2511–2523. [CrossRef]

51. Fraser, R.S.; Kaufman, Y.J. The Relative Importance of Aerosol Scattering and Absorption in Remote Sensing. *IEEE Trans. Geosci. Remote Sens.* **2007**, *23*, 625–633. [CrossRef]

52. Knippertz, P.; Todd, M.C. Mineral dust aerosols over the Sahara: Meteorological controls on emission and transport and implications for modeling. *Rev. Geophys.* **2012**, *50*, RG1007. [CrossRef]

53. Tesfaye, M.; Sivakumar, V.; Botai, J.; Tsidu, G.M. Aerosol climatology over South Africa based on 10 years of Multiangle Imaging Spectroradiometer (MISR) data. *J. Geophys. Res. Atmos.* **2011**, *116*, D20216. [CrossRef]

54. Wang, Y.; Wang, J.; Levy, R.C.; Xu, X.; Reid, J.S. MODIS Retrieval of Aerosol Optical Depth over Turbid Coastal Water. *Remote Sens.* **2017**, *9*, 595. [CrossRef] [PubMed]

55. Mei, L.; Xue, Y.; Xu, H.; Guang, J.; Li, Y.; Wang, Y.; Ai, J.; Jiang, S.; He, X. Validation and analysis of aerosol optical thickness retrieval over land. *Int. J. Remote Sens.* **2012**, *33*, 781–803. [CrossRef]

56. Martins, J.V.; Tanré, D.; Remer, L.; Kaufman, Y.; Mattoo, S.; Levy, R. MODIS Cloud screening for remote sensing of aerosols over oceans using spatial variability. *Geophys. Res. Lett.* **2002**, *29*, MOD4-1–MOD4-4. [CrossRef]